A Final Grant Report to the BC Ministry of Water, Land and Air Protection (WLAP)

South Central BC

Air-Quality Ensemble Forecast Research

Research Period: 1 Jan - 31 March 2003

Principal Investigator: **Dr. Roland Stull**, Professor
Geophysical Disaster Computational Fluid Dynamics Ctr.
Dept. of Earth & Ocean Sciences, UBC
6339 Stores Rd., Vancouver, BC V6T 1Z4
604-822-5901 , fax 604-822-6088 , rstull@eos.ubc.ca

Researchers: **Dr. Terry Clark**, Visiting Scientist & Co-Investigator
Ms. Xingxiu Deng, MC2 model expert
Ms. Trina Cannon, Verification expert
Ms. Alyssa Gloeckler, Analyst
Mr. Luca Delle Monache, Air Quality expert

System Administrators: **Mr. Henryk Modzelewski**
Mr. George Hicks

Contents: page

6 May 2003

Executive Summary

Activities

The Canadian Mesoscale Compressible Community Model (MC2) was run at the University of British Columbia (UBC) to produce high-resolution weather forecasts for the Okanagan and Kamloops regions. Although five one-way nesting levels were used (with grid spacings of 108, 36, 12, 4, and 2 km) to make the forecasts, only the two finest grids were the focus of this study.

Three periods were forecast: a 2-month operational, real-time period (1 February - 31 March 2003), and two case study periods (summer: 12 – 26 June 2002, and winter: 29 January – 10 February 2003). These periods were selected by WLAP to allow comparison with other model runs and with special field data, with the strategic goal of creating higher-quality meteorological input to air-quality models.

Research was conducted toward developing an even higher-resolution model called the Weather-Fire Integrated System (WFIS). The WFIS model was run with two nests: 2 km and 1 km grid spacing. The 2 km nest received its initial and boundary conditions from the MC2 run at 2 km. Experiments were done to improve this coupling.

Results

For summer and winter cases using MC2, the 2 km resolution weather map is better than 4 km, showing more realistic surface winds that capture the mountain/valley and anabatic/katabatic winds and channeling. The forecast soundings for both resolutions show smooth but realistic features above the boundary layer; however, the boundary-layer forecasts show significant errors in both mixed layer depth and temperature.

Verification statistics of model forecasts against observations from roughly 15 surface weather stations near Kamloops and Kelowna show that both models have relatively small errors. Their verification statistics are similar (often sharing similar biases and error variances), with the finer grid have slightly larger verification errors. This characteristic has also been observed by other numerical modeling groups, and is caused by bad weather analyses advecting over the verification region from upwind over the Pacific Data Void.

The MC2/WFIS coupling experiments were successful, and showed that: density weighting (i.e., momentum coupling) gives similar results as wind coupling; one-way and two-way grid interaction gives similar results; fine-scale features from the fine mesh must be horizontally filtered out before entering the coarser mesh; higher-resolution orography in WFIS causes 30% increase in local vertical velocities; and MC2 errors caused by the Pacific Data Void propagate without reduction into WFIS forecasts. The stage is set for much finer grid resolution (100s to 10s of meters) WFIS forecasts during future grants.

Ensemble fine-resolution, real-time weather forecasts are now possible for the complex terrain of BC, and can be used as input to air quality models for WLAP.

1. Discussion of Forecast Quality from 2 km and 4 km Grids

a. Introduction

Maps of the 4 and 2 km grid domains are shown in Fig. 1.1. An advantage of coarser grids are that they require fewer computations, thereby allowing forecasts over larger domains and longer time periods. However, coarser grid spacings require smoothed terrain to satisfy air-mass conservation, which leads to lower mountain-top heights, higher valley–floor heights, and gentler slopes that can cause forecast errors. For example, a valley forecast may chronically be too cold, because the model is actually forecasting for the conditions at a higher elevation. Other meteorological factors, such as wind speed and direction, precipitation rate, the speed at which low-pressure systems move through an area, etc., are also affected by topography. Also, the influences of smaller-scale, unresolved phenomena (e.g., turbulence, small clouds, trees, etc.) must be approximated.

Finer grids can better resolve the topography and the topographically-induced weather. The also deterministically forecast more of the smaller scale phenomena (more of the clouds, larger turbulent eddies, etc.). As grid spacing is reduced, time steps taken by the model must also be reduced to ensure computational stability. Hence, fine-grid models can be run for only shorter periods and smaller domains, because of their intense computational demand.

A good compromise, as run at UBC, is to nest finer grids inside coarser grids. That way, the coarser grids capture the big-picture for larger timer periods, while the finer grids nested inside focus on the region of interest. After each grid is initialized and run, the first 3 hours of the forecast are discarded because the model is still reaching a balanced state. The remaining hours are used to initialize, and provide boundary conditions, to the next finer grid. Thus, each forecast is started 3 h after the previous one, as shown in Table 1.1 .

Table 1.1. Forecast duration for nested MC2 grids.

Grid Spacing (km)	Start Time (UTC)	Fcst Duration (h)	End Time (UTC)
108	00	60	00 UTC + 60h
36	03	57	00 UTC + 60h
12	06	54	00 UTC + 60h
4	09	51	00 UTC + 60h
2	12	27	00 UTC + 39h

The first 3 hours of output from the 2 km grid is discarded, and the remaining 24 hours are saved. Thus, the saved forecast period from the 2 km grid is a 24 h period starting at 15 UTC (7 am PST or 8 am PDT) each day. This process is repeated day after day, to sequentially build-up a multi-week period of high-resolution weather forecasts, as can be used as input to air quality models. These forecasts were provided to WLAP on hard disk, in the format described in Appendix A.

b. Winter Case Study: 28 January to 10 February 2003

The winter of 2003 was relatively dry, and warm in southwest BC due to predominantly zonal flow over the northeast Pacific. Many of the winter storms were deflected northward around BC. During the period of this 2-week winter case study this general weather pattern persisted.

Weather Maps

Sea-level pressure forecasts from both the 4 km and the 2 km grids showed a low-pressure system moving towards British Columbia, but then being deflected northward. This resulted in an initial rapid increase in pressure, followed by continuous high pressure during 1-10 February. The low-pressure system moved at the same speed in both grids, and the pressure rose and fell similarly in both grids. The difference between the two forecasts was not in the movement of system, but in the level of fine detail present in the forecast. Though each grid produced the same over all pressure structure, the 2 km mesh added finer detail within this structure, and resulted in a more precise forecast. To examine this further we will compare the 24 hour forecasts from the two grids initialized from 00 UTC on 1 February 2003.

Fig. 1.2 shows sea-level pressures from the two runs. Clearly, the finer-resolution domain showed more detail in the pressure pattern, but it is difficult to use these pressure details to anticipate wind directions because of the complicating influences of terrain. As will be shown later for the summer case, surface winds are a more useful output product for the mesoscale.

Figs 1.3 a and b show plots of the horizontal wind streamlines at roughly 1.7 km above sea level. Both forecasts captured the large-scale flow, namely, prevailing winds over the domain were the same (northwesterly to west northwesterly), and diffluence and confluence occurred in the same areas (for example diffluence is evident between 120-122 degrees W, and 48-49 degrees N, as streamlines are spreading out from each other). However, since the 2 km domain provides finer resolution, it captured more details of the flow at the mountainous coast of British Columbia. In the 4 km grid notice the smooth streamlines over the ocean became disturbed when they move over land. This disturbed flow continued downwind, and in the interior of British Columbia, the 2 km was better at capturing this flow, for example look between 118 and 120 degrees W and 50 and 51 degrees N. There is a region in the 2 km output where the winds are northwesterly, and there is a small amount of diffluence occurring in the region, which is evident in the 2 km output.

Finally, compare the surface temperature outputs for both grids (Fig 1.4 a & b). Once again both grids captured the same large-scale temperature distribution. As in the other cases, the 2 km grid primarily enhanced the detail of temperature distribution. However, the region between 49 and 50 degrees N, and 120 and 122 degrees W, in the 4 km grid contained three distinct areas of warmer temperature, while the 2 km grid showed a contiguous area of warmer temperature. Also, the area of warmer temperature

in the 2 km output appeared to be over a smaller area than in the 4 km. This example shows that the added detail provided by the smaller grid mesh may result in forecasts that show more homogeneous results than the coarser grid. The increased precision of the 2 km grid is more than an intuitive change in detail, and often demonstrates an improvement in forecast accuracy.

Soundings

Soundings for Kelowna (49.93 N, 119.40 W, and, 456 m MSL) are shown in Fig. 1.5 a and b. The 24 hour output from both the 4 km and 2 km grids, valid at the 00 UTC 2 February initialization, are plotted on Skew T diagrams along with the observational sounding valid at 2325 UTC 1 February. The observations showed a humid layer between 80 and 60 kPa. Above this the temperature decreased at a rate that was close to the saturated adiabatic lapse rate. Dryer air was aloft, as the dew-point temperature dropped suddenly at 50 kPa, and 35 kPa. At the surface a small inversion was present.

The 4 km grid sounding (Fig 1.5a) showed that the model captured some of the features of the observations. The moist layer existed, beginning as it does in the observations, at 80 kPa. However, the forecast moist layer was shallower, with the dew point temperature beginning to drop at 70 kPa. The dry layer above this was also drier in the forecast, with a dew point depression of 10 degrees C at 60 kPa (8 degrees C higher than in the observations). Also, this dry layer was located higher in the observations than in the forecast. Between 50 kPa and 40 kPa the model captured the environment lapse rate and temperatures well. For the dew point temperature, however, it was less accurate, predicting much cooler dew point temperatures between 60 and 50 kPa than occurred. The model was also fairly poor at forecasting temperatures in the boundary layer. The inversion capping the boundary layer was 200 - 300 m too high in the forecast, and the average temperature in the mixed layer was about 5 C too cold in the forecast. These are large errors in a part of the domain that is very important for air-quality forecasts.

The 2 km grid sounding (Fig 1.5b) was similar to the 4 km sounding in that it captured the main features of the observations. Both the dry and humid layers were present, however, the dry layer was slightly higher than in the 4 km sounding, and therefore more accurate. Once again, the forecast did a good job of capturing the lapse rate of temperature between 60 kPa and 40 kPa, with the forecast temperatures being on average, slightly warmer. An advantage of the 2 km grid sounding can be found at the lower heights. The 2 km sounding began at a lower height (due to better topography resolution), and attempted to capture some of the near surface level inversion characteristics. While the forecast temperatures remain colder than the observed temperatures, they were slightly warmer than in the 4 km grid sounding. Also, the model accurately forecasted the presence of a surface level inversion, although it predicted an inversion that was much deeper and stronger than the observed.

From an analysis of these soundings we find that both the 2 km and 4 km grid forecasts were able to accurately forecast the features of temperature soundings, except in the boundary layer. The 2 km forecast output was slightly more accurate overall, and produced a slightly better boundary layer forecast.

c. Summer Case Study: 12 – 26 June 2002

The summer case study period was dominated by weak pressure gradients, and variable winds. On 12 June, the dominant winds were from the east, with variable winds throughout central BC. By 15 June winds shifted to westerly, as a weak center of high pressure moving northeast approaches the coast of Vancouver Island. There were no major weather systems affecting the region over this time period, resulting in near constant pressure over most of Southern BC.

Weather Maps

The model output for this case study period shows a similar relationship between the 4 km and 2 km grid as was found for the winter case. The main difference is again the finer detail of the 2 km grid.

For high-resolution mesoscale meteorology in complex terrain, winds are a more useful output product than pressures, particularly near the surface. Figures 1.6a and b show the 4 km and 2 km grid output of surface winds and convergence (shaded) for the 24 hour forecast of the model initialization at 00Z 15 June 2002. Notice that both grids forecast the same wind flow patterns. At Kelowna, winds were southerly, and at Kamloops they were southeasterly.

Both grids also agreed on the locations of convergence (for instance, the area south of Kamloops is a location of a line of convergence). The terrain-forced winds through the valleys are more clearly visible in the 2 km output (Fig. 1.6b), as the higher level of detail better captured certain terrain flow features that were missing in larger grid outputs. In this way, the finer grids better capture the channeling of winds in valleys, and the anabatic (warm upslope) and katabatic (cold downslope) circulations typically found during fair weather.

Soundings

The observed sounding, made at 23:18 UTC on 14 June 2002, is plotted in Figs 1.7 a and b. It shows an environmental lapse rate that was close to the dry adiabatic lapse rate existed from the surface to 65 kPa. This represents an exceptionally deep mixed layer -- roughly 3 km deep. Above the boundary layer, the lapse rate was between the dry and saturated adiabatic lapse rates. A moist layer existed around 60 kPa; otherwise the air was dry. Two small upper-level inversions were present at 52.5 kPa and 60 kPa. The sounding showed a shallow unstable layer near the surface, followed by a neutral atmosphere up to 65 kPa, and conditionally unstable conditions aloft.

The 4 km grid (Fig 1.7a) produced a fairly accurate sounding. Though the near-surface temperatures were too cold, and the upper-air temperatures were too warm, the lapse rate was close to that of the observations, especially above 50 kPa. The model also forecast the moist layer, and predicted the relative humidity at this layer close to what was observed. However the layer was slightly lower and shallower in the forecast. The forecast did not show the small inversions at 52.5 and 60 kPa, near the top of the

boundary layer. The boundary-layer forecast is again problematic. The 4 km grid shows a very shallow mixed layer capped with a weak inversion, with a nearly adiabatic layer above it, rather than the single deep mixed layer that was observed.

The forecast temperatures from the 2 km grid (Fig 17b) were too cool at lower levels, and too warm at higher levels. The humid layer at 60 kPa was present, however the small inversions were also missing in the 2 km sounding. The 2 km was slightly poorer at forecasting upper level temperatures than the 4 km grid, with temperatures higher than both the 4 km grid and observations. The boundary layer was worse in the 2 km grid than in the 4 km grid, with a stronger inversion capping a mixed layer that was much too shallow compared to the observation.

2. Verification Statistics: Comparison Between Model Output and Surface Observations

Verification statistics for the 2 and 4 km grid output for the two-month operational forecast period between 1February and 31 March 2003 are listed in Appendix B. These statistics were calculated by comparing surface observations at 13 stations near Kelowna, and 15 stations near Kamloops, to the corresponding model forecasts. The variables verified include temperature, surface and mean-sea-level pressure, precipitation, relative humidity, wind speed, and eastward and northward wind components.

Verification statistics include mean error (also known as forecast bias), mean absolute error (which indicates forecast accuracy), error variance (which indicates how scattered errors are around mean), root mean square error (RMSE, zero is best), correlation between forecast and observation (1.0 is best), slope of the best fit line between forecasts and observations, forecast variance, and observation variance.

For illustration, a brief summary of 24-35 h bias (i.e., mean error), extracted from Appendix B, is given in Table 2.1 .

Table 2.1 . Forecast bias (mean error) during the 24-35h portion of the forecast.

	Kamloops		Kelowna	
Variable	**4 km grid**	**2 km grid**	**4 km grid**	**2 km grid**
Temperature (C)	-3.87	-4.15	-4.95	-5.48
Sfc. Pressure (kPa)	-3.25	-2.89	-1.05	2.83
Hr. Precipitation (mm)	-0.02	-0.02	-0.06	-0.06
Relative Humidity (%)	2.86	4.25	13.25	17.57
Wind Speed (km/h)	-1.68	-2.23	-3.07	-3.75
U-wind (km/h)	0.09	-0.39	-0.72	-1.02
V-wind (km/h)	0.05	-0.04	1.32	0.96
MSL Pressure (kPa)	0.03	0.06	0.27	0.33

As has been reported by other mesoscale modelers, verification statistics for the highest-resolution domain are often worse than for coarser-resolutions. This is true even though weather maps for the finer grids (from section 1) show more realistic, fine-scale weather features. Both Cliff Mass' NWP group at the University of Washington, and Roland Stull's NWP group at UBC, have verified that one large reason for these errors is the Pacific data void. Namely, errors in the large-scale flow direction as advected in from upstream over the Pacific, when imposed on fine-scale models, cause the fine-scale weather features to appear in slightly the wrong places. This often results in local flow directions being opposite to what is observed. The ultimate solution to this problem is better upstream weather observations over the Pacific Data Void, which is beyond the scope of this research.

For certain variables, both grids had similar results. The hourly precipitation forecast at Kamloops and Kelowna is one example, where both grids showed the similar level of accuracy. Both grids also had zero error variance, and both grids showed a negative bias in their forecasts, indicating that they forecasted less precipitation than occurred.

For some variables, grid performance was related to the location of the forecast. For example, the 2 km grid did a better job of predicting winds in Kamloops. For wind speed, the 2 km grid was more accurate, though it had a larger bias than the 4 km grid. The U and V wind component forecasts were also more accurate at the 2 km grid. Meanwhile, the 4 km grid was more accurate, had a smaller bias, and smaller variance for winds (both speed and component speeds) in Kelowna.

The 4 km also showed slightly better results for some variables, such as for surface pressure and relative humidity. This may be due to the fact that the 2 km grid initialization occurs later than the 4 km grid. Therefore, when comparing the 12-23 hour verification statistics, the 2 km grid may not be fully balanced, resulting in errors. Often, the 2 km grid results showed a marked improvement in accuracy with time. Sometimes this would result in the 2 km grid accuracy surpassing the 4 km grid accuracy by the end of the run. One example of this is surface air temperature at both Kamloops and Kelowna. At Kamloops, the 4 km grid had a lower mean error (-4.28 degrees C compared to – 4.5 degrees C), absolute error (4.5 degrees C compared to 4.68) and error variance (15 to 16) for 12 to 23 hours. However, the 2 km grid became more accurate by 36 to 47 hours (the mean absolute error for 4 km grid was 4.53 degrees C compared to 3.91 degrees C for 2 km grid). The same pattern is seen at Kelowna. Other variables, where the 2 km accuracy did not surpass the 4 km accuracy by the end of the run it still showed a larger improvement in accuracy with time than the 4 km domain.

While both grids showed higher accuracy for different forecast variables, in general the errors being made by the forecasts were similar in nature. For instance, both grids have a cold bias in surface temperature forecasts. Also, the magnitude of errors was often very close, indicating a good agreement between the forecasts being made for both grids.

3. High Resolution WFIS Modelling Research

by *Terry L. Clark*
In collaboration with Luca Della Monache, and Roland Stull

a. Summary

This report describes the work to-date using the Weather Fire Integrated System (WFIS, also known as the Clark model) to predict fine scale weather over the Okanagan Valley. A major part of the research is devoted to how the MC2 forecast data is used to initialize and force the WFIS code at its outermost lateral boundaries. Projecting horizontal winds versus horizontal momentum was tested and found to give very similar results. The WFIS model was run for a specified time of either 3 or 6 hrs.

A number of the 3 hr WFIS forecasts were compared with the MC2 forecasts to evaluate differences between the two systems. At similar resolution and physical forcing, the results showed that the differences between the two models were acceptable and relatively minor for the case considered.

Other comparisons show that the WFIS code gives similar results for one-way and two-way interaction between its 2 km and 1 km grid resolution nests when the higher resolution topography is simply interpolated from the coarser nest, i.e. has the same resolution. This is a necessary result because we should not expect significant differences unless the higher resolution nest is actually capturing higher resolution physics such as physical topographic forcing. However, we found that if we did not filter the highest frequency modes in the fine grid nest near its outflow boundaries then the two-way interaction showed a weak numerical instability. Other than eliminating a weak numerical instability we showed that the high frequency filter had a very minor effect on the forecasts.

Another aspect of the research is testing the effect of using higher resolution topography in the WFIS code compared that used in the MC2. For the case considered the differences showed larger amplitudes in the mountain induced vertical velocity patterns by about 30 %. Finally a comparison between the MC2 and WFIS predictions at 3 pm (local) for Kelowna is shown. The MC2 forecast shows some significant differences suggesting the model has incorrectly predicted the location of a frontal pattern at this time. As discussed earlier, this is likely due to bad upstream data from over the Pacific Data Void. Since the WFIS model takes its initial and boundary condition data from the MC2 its 6 hr forecast showed very similar comparisons. In conclusion a number of suggestions are proposed for future research beyond what time allowed for this work.

This is the second research report on the WLAP project and the material presented herein follows that of the previous report, dated 7 March 2003.

b. Goals

The goal of this research is to understand the effects of driving a high-resolution limited area model with initial and boundary conditions taken from a lower resolution model. In our case the high resolution model is the Weather Fire Integrated System (WFIS) that will take its boundary conditions from the MC2. We explore different methods of projecting the MC2 data onto the WFIS grid.

We also explore the effect of projecting the MC2 data on the WFIS model when the WFIS model is using higher resolution topography. The fact that the WFIS topography needs to be internally consistent means it is a non-trivial problem to allow the coarse nest of the WFIS model to have the same topography as the MC2 data. In this report we use the simple approach of using an abrupt change between the WFIS and MC2 topographies rather than testing variation approaches to minimizing the change.

c. MC2 Data Ingestion into the WFIS code

In the 7 March 2003 report we were still using the 4 km MC2 data. By the end of March Xingxiu Deng had successfully converted to using 2 km MC2 data. Following this we ran a series of 3-hour simulations using the 2 km MC2 forecast data and compared the WFIS predictions with those from the MC2 to evaluate the direct effect of the differences between the WFIS and MC2 models, as it seems logical to establish the degree to which the WFIS and MC2 models are consistent under similar physical forcing conditions.

Table 3.1 describes a series of WFIS experiments using 2 km MC2 data for initial and boundary conditions. All of these experiments used two nests with the inner nest using 1 km horizontal resolution. All experiments started at 9 am local time or 05 UTC and were integrated forward to local noon.

The series of experiments, shown in Table 3.1, were run for only 3 hours to facilitate quick turn around on the simulations and subsequent analysis. It turned out to be somewhat difficult and time consuming to understand the reasons for the differences between the WFIS and MC2 model predictions. The experiments shown represent only a fraction of those considered. I felt it was important to understand the differences particularly because the WFIS code is to take its initial and boundary conditions from the MC2. Longer integration times are considered for the comparison between the model data (both WFIS and MC2) and observations.

Two options exist in the WFIS code for the projection of the input data from MC2. One directly interpolates the horizontal velocity components (U, V) onto the WFIS grid using the option ρ_{wgt} =0 whereas the second projects (ρU, ρV) using the density, ρ, from the MC2 data (ρ_{wgt} =1). After interpolation, (ρU, ρV) are divided by the appropriate density of the WFIS model.

Table 3.1. Description of MC2-WFIS comparison experiments.

Experiment WFIS file	MC2 File	ρ_{wgt}	TOPO	Layer Interaction	Horiz-Filter	Integration Period	Dt (s)
WLAPK3	MC2LW3	1	MC2	One-Way	Off	3 hrs	20./10.
WLPFK3	MC2WL3	1	MC2	One-Way	On	3 hrs	20./10.
WLAPK4	MC2WL4	0	MC2	One-Way	Off	3 hrs	20./10.
WLAPK5	MC2LW3	1	MC2	Two-Way	On	6 hrs	20./10.
WLAPK6	MC2LW6	1	High	Two-Way	On	6 hrs	

d. Effect of Density Weighting (momentum vs. wind ingestion)

Experiments WLAPK3 (using ρ_{wgt} =1 to create MC2LW3 initial condition files) and WLAPK4 (using ρ_{wgt} =0 to create MC2LW4 initial condition files) test the effect of density weighting when projecting the initial and boundary condition data onto the WFIS model. Before showing results from the simulations we show the orography taken from the MC2 model used for these experiments. Figure 3-1 shows the orgoraphy interpolated from the MC2 data onto the WFIS grid at (a) 2km and (b) 1 km horizontal resolution. The actual model resolutions are $\Delta y = 2(1)$ km and $\Delta x = 2(1)$ km at 60 degrees North for nests 1 (2).

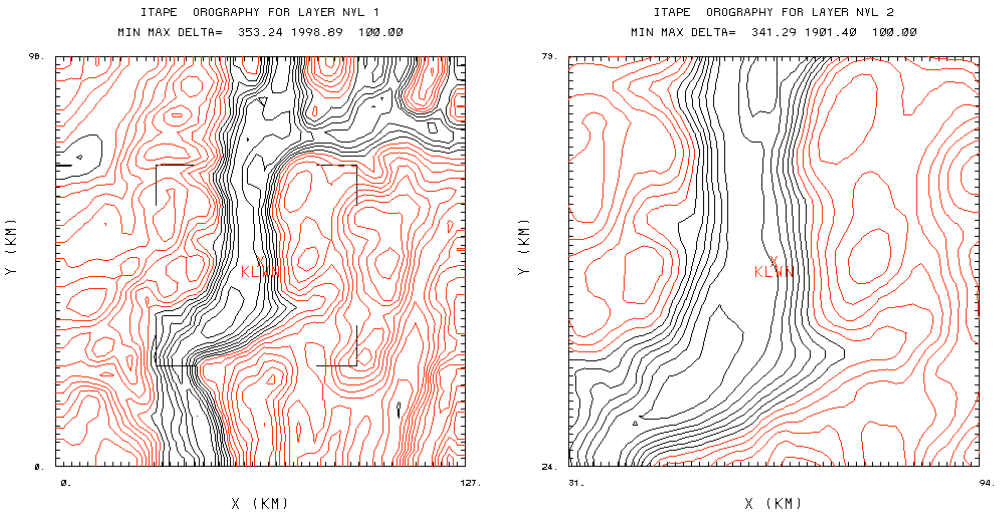

Figure 3-1 – Orography from the 2 km MC2 data used in experiments WLAPK3, K4 and K5. (See Table 3.1). The contour interval is 100 m and red contours show elevations higher than 1000 m MSL.

Figure 3-2 shows vertical velocity, w, at four heights for WLAPK4 and MC2WL4 (ρ_{wgt} = 0). The 3 hr prediction from WFIS is on the left whereas the MC2LW4 projected data at local noon is on the right. The heights shown are 0.189, and 3.70 km AGL. At

both the lower and higher level we see the strong up- and downdrafts at inflow correspond reasonably well between the WFIS and MC2. Other regions also agree with respect to the general structure of w. There are, though, substantial differences between the details of the fields where the WFIS has larger amplitudes of w by a factor of 2 to 3.

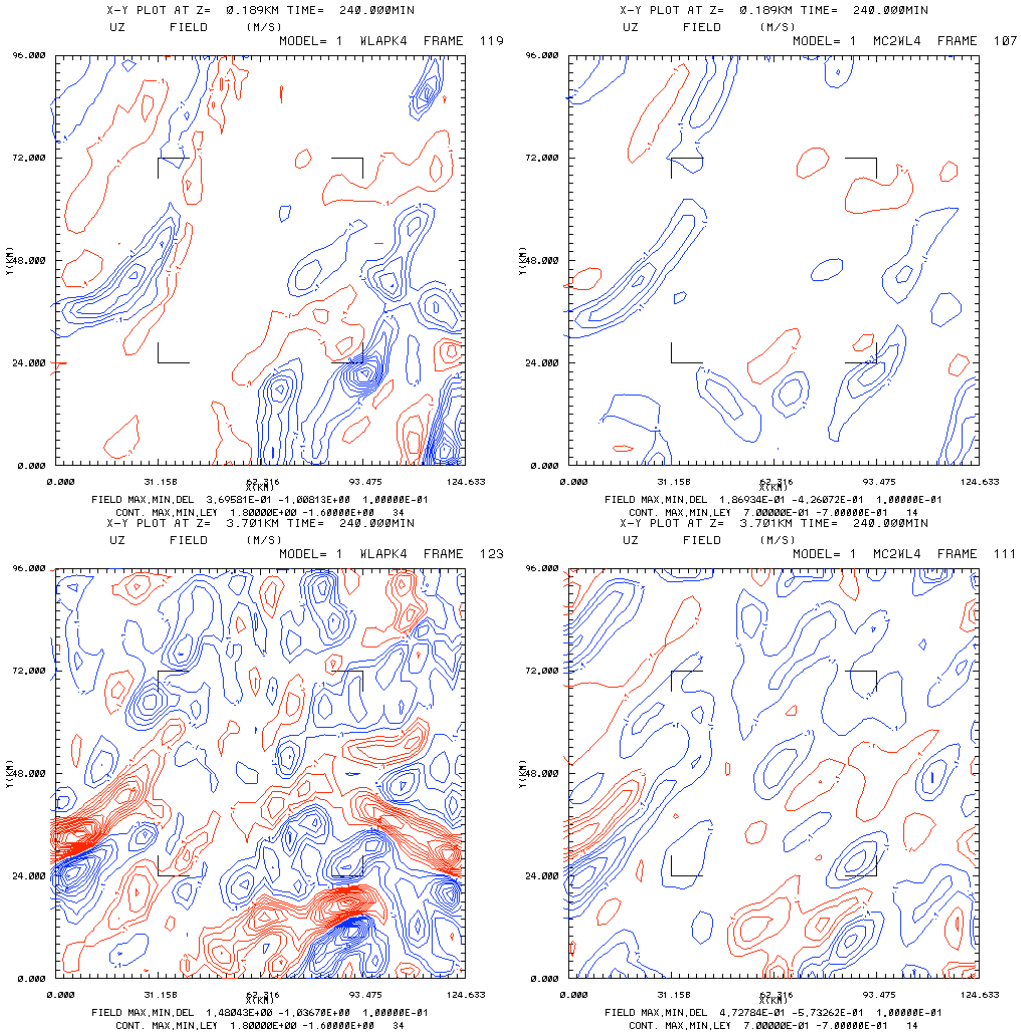

Figure 3-2. Vertical velocity at the heights of 0.189, and 3.70 km AGL are shown for the WLAPK4 experiment after 3 hours of integration. MC2WL4 (shown on the right) is the MC2 data projected onto the WFIS grid using $\rho_{wgt} = 0$. The contour interval is .1 m/s throughout. Red is positive whereas blue is negative.

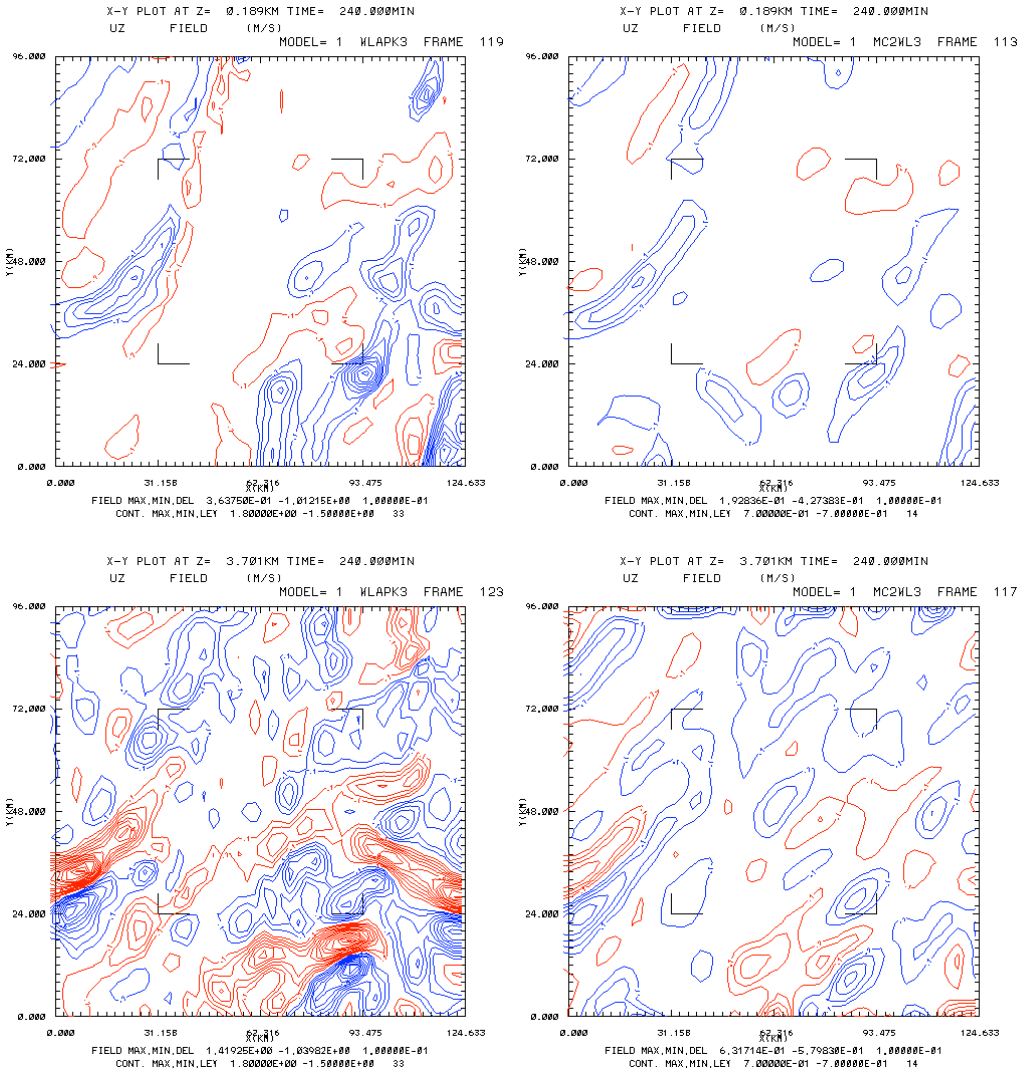

Figure 3-3. Vertical velocity at the heights of 0.189, and 3.70 km AGL are shown for the WLAPK3 experiment after 3 hours of integration. MC2WL3 (shown on the right) is the MC2 data projected onto the WFIS grid using $\rho_{wgt} = 1$. The contour interval is .1 m/s throughout. Red is positive whereas blue is negative.

Figure 3-3 shows the same w fields as in Fig. 3-2 but for WLAPK3 (MC2WL3) experiment. The comparison is almost identical indicating that density weighting had only a minor effect. This result suggests that the differences between the anelastic density profile and the density for the MC2 model are not a cause for concern. Because of some earlier erroneous analysis we had thought that the density weighting case was much closer to the MC2 case instead of almost identical. Because of this we ended up using $\rho_{wgt} = 1$ for the remaining experiments. We also show the comparison at the same two heights for u (Fig. 3-4), v (Fig. 3-5) and θ (Fig. 3-6) for WLAPK3.

Figures 3-4 through 3-6 show strong similarities between the WFIS and MC2 predictions of U, V and θ at z = 0.211 and 3.90 km AGL. One of the differences is that WFIS predicts slightly stronger gradients than the MC2. It is perhaps these stronger gradients that led to a low level (0.211 km AGL) south wind component in the Okanagan compared to the MC2 prediction of an extremely weak northerly component at that level. Another difference is that the WFIS shows a very slight bias towards warmer temperatures of about 1 degree K.

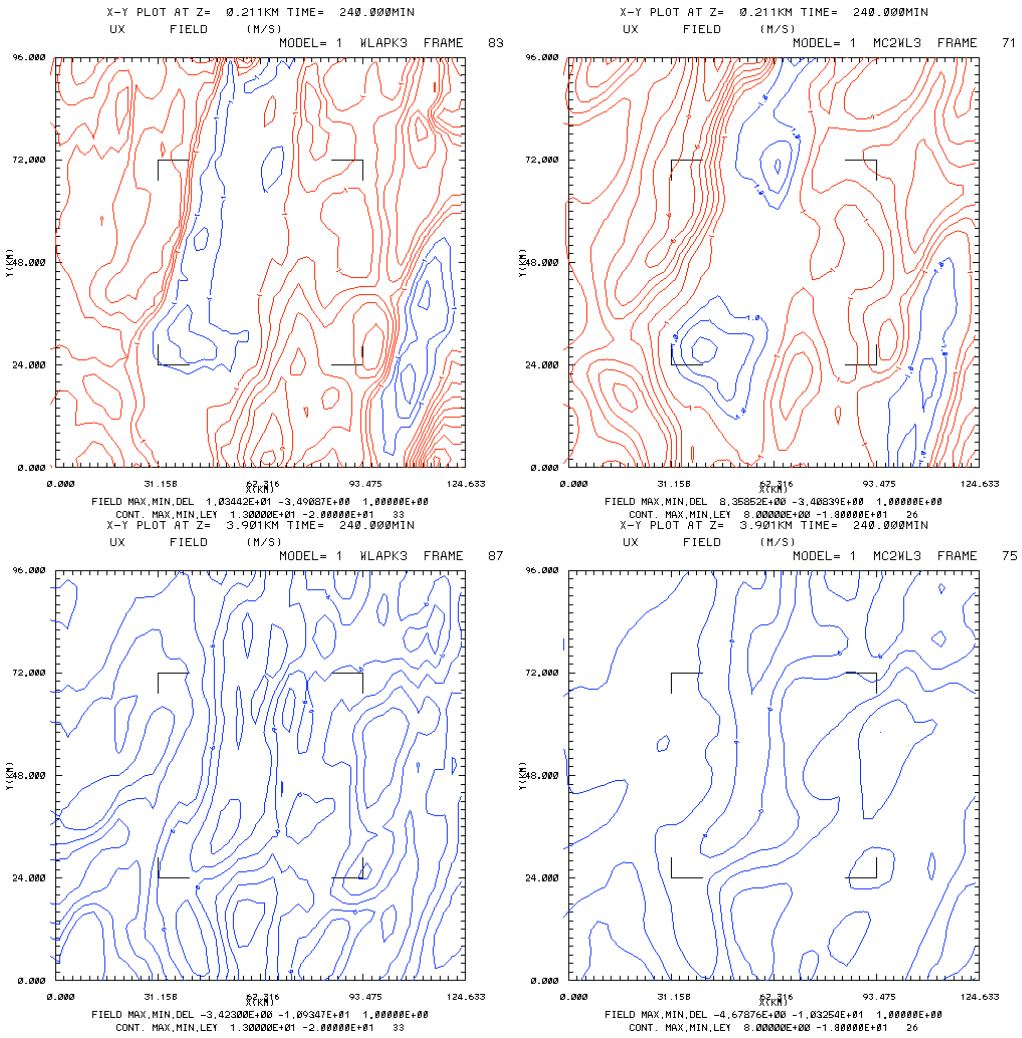

Figure 3-4. U at 0.211 and 3.90 km AGL. Contour interval is 1 m/s with red (blue) positive (negative). WLAPK3 is on the left and MC2WL3 on the right.

Experiment WLAPK3 is as close a prediction to the MC2 model that we should expect since we not only used the MC2 smoothed orography but also did not allow the effects of grid refinement feed back onto the 2 km data. Before showing the effect of grid refinement, we first show the effect of filtering the highest frequency (or 2 delta) modes.

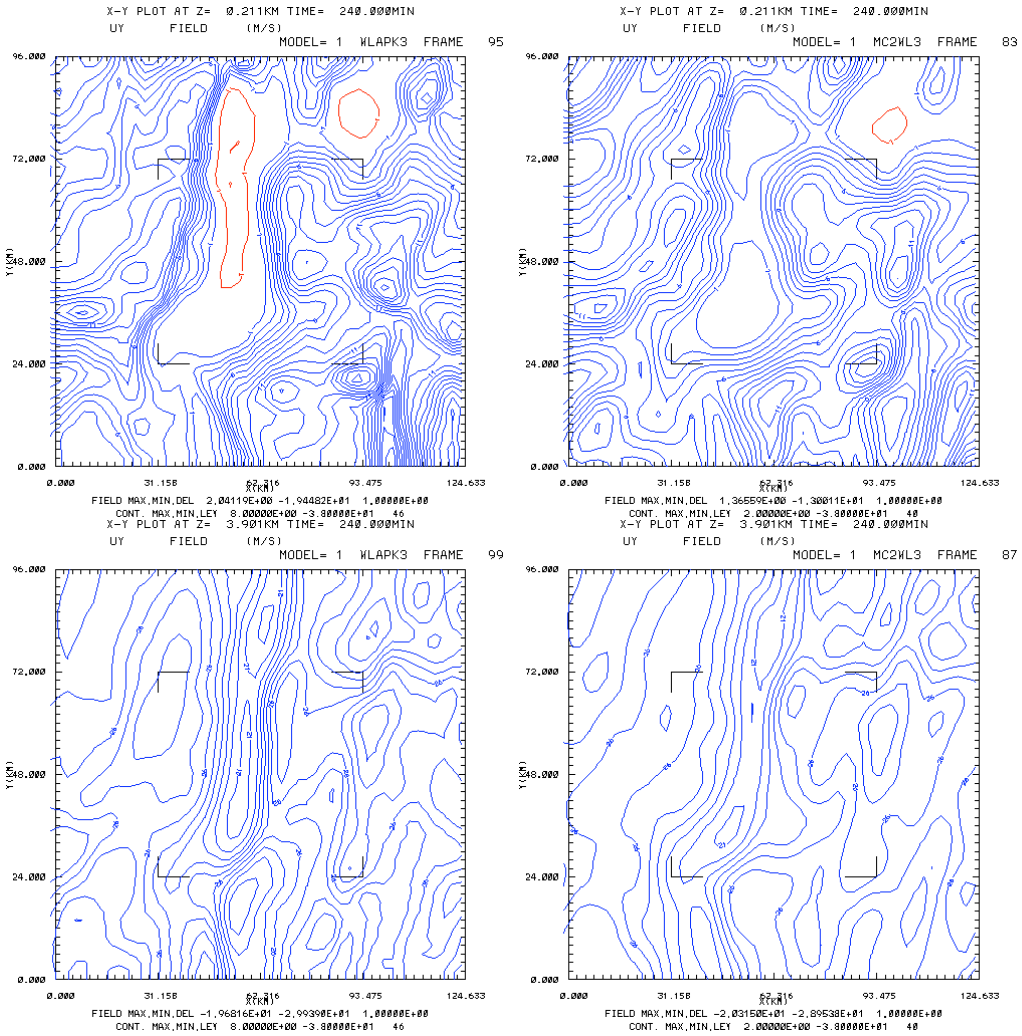

Figure 3-5. V at 0.211 and 3.90 km AGL. Contour interval is 1 m/s with red (blue) positive (negative). WLAPK3 is on the left and MC2WL3 on the right.

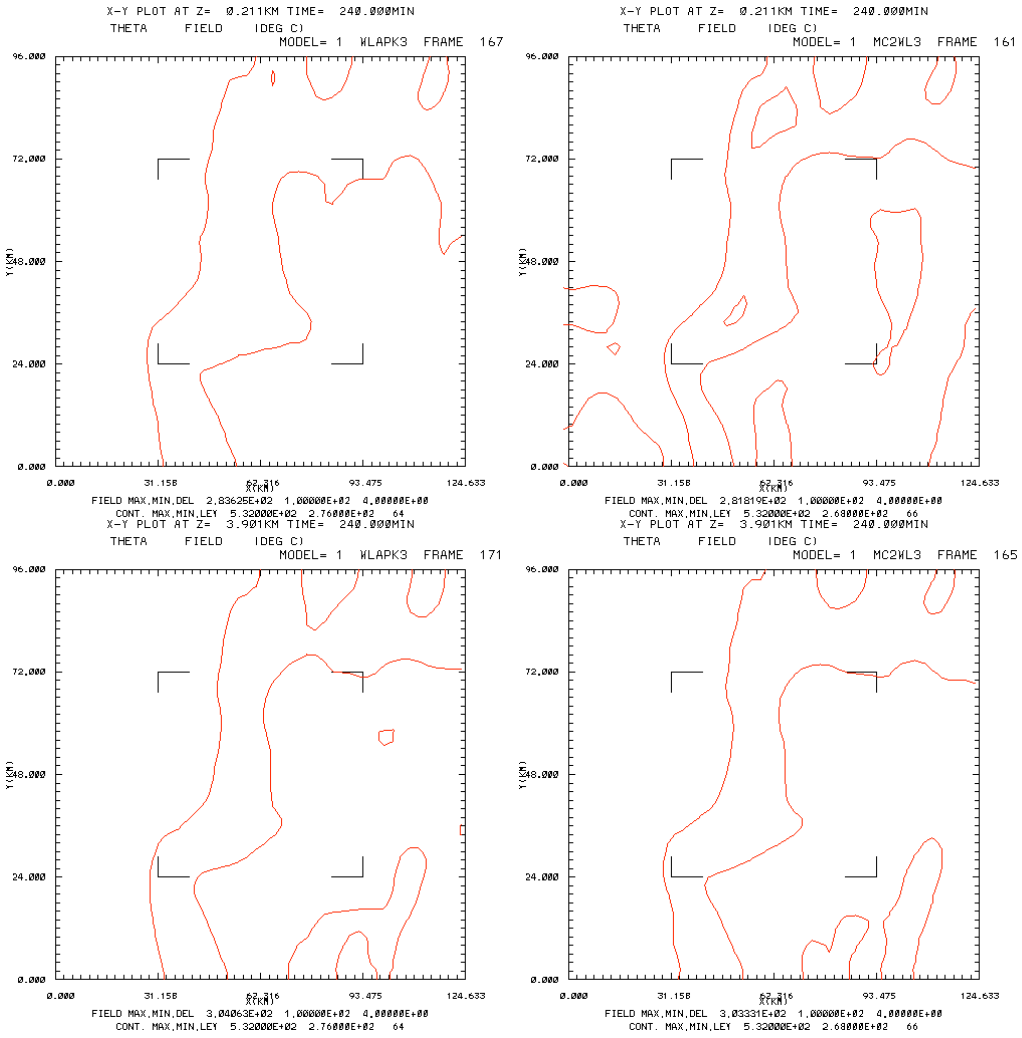

Figure 3-6. θ at 0.211 and 3.90 km AGL. Contour interval is 4 K with red (blue) positive (negative). WLAPK3 is on the left and MC2WL3 on the right.

e. Effect of Horizontal Filters

In the WFIS code we employ horizontal filters that damp two-delta modes (i.e. numerical noise). The filter is designed as a combination of ∇^2 , ∇^4 and ∇^6 and are applied only to the U,V and W fields along ζ surfaces. The design of the filter is typically 3 rows of ∇^2 nearest the lateral boundaries followed with 2 rows of ∇^4 filtering and the remaining interior is treated with ∇^6. The ∇^6 has a very sharp $2\Delta x, 2\Delta y$ cutoff which is why we went to this order. The amplitudes used were 0.5, 0.4 and 0.2, i.e. 0.5 of the $2\Delta x, 2\Delta y$ would be damped in one time-step by the ∇^2 and 0.4 by the ∇^4 and 0.2 by the ∇^6 filter. *This horizontal filtering is important when considering the two-way interactions because without the effect of damping high*

frequency waves (i.e. two and three delta modes) near the boundaries of the inner (high resolution) layer we develop numerical instabilities. The smaller waves that are not resolved by the coarse grid must be damped rather than allowed to reflect and build in amplitude. If we consider only one-way interactions we do not obtain any numerical growth, i.e. this is a result of the two-way interaction.

Note that the previous comparison between the WFIS and MC2 was for one-way interaction and with the horizontal filters off. When we turn the horizontal filters on for even the one-way interaction we will see some minor differences resulting from damping the highest frequency modes. For this reason we ran two further experiments with one-way interaction and with the horizontal filters active. These experiments show the effect of the filtering as well as provide experiments that we can use to assess the effect of two-way interaction and resolution of the orography. We show a comparison between WLPFK3 and WLAPK3 to see the effect of the horizontal filter on the w field.

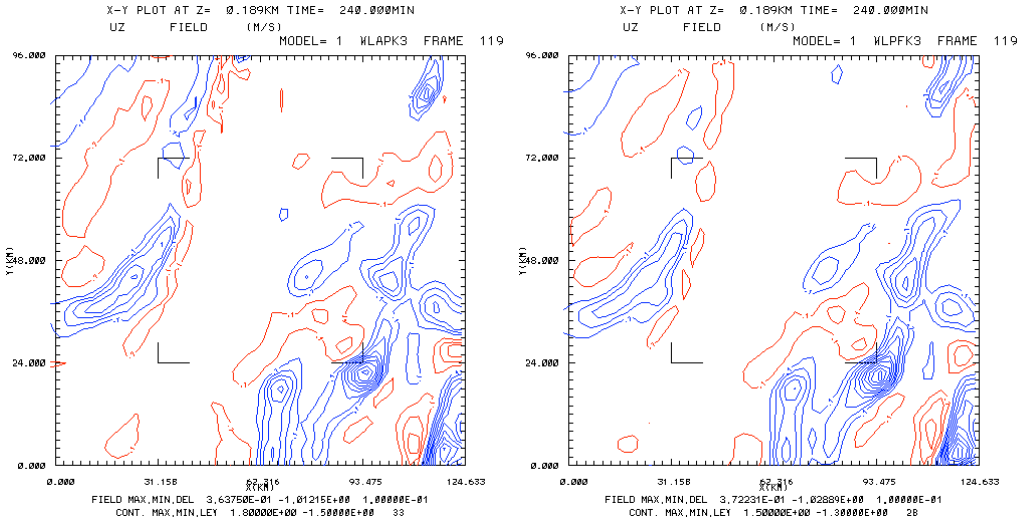

Figure 3-7. *w* for WLAPK3 and WLPFK3 at t = 3 hrs (local noon) into the simulation at z = .189 km AGL. Shows effect of using horizontal filter.

Figure 3-7 shows a comparison between WLAPK3 (no filter) and WLPFK3 (with horizontal filter). The main effect is a small decrease in amplitude of the *w* modes. In the comparisons that follow we use WLPFK3 for the comparisons to limit the model differences.

f. Effect of Two-Way Interaction

It is important to note that the two-way interaction required the horizontal spatial filters to be active to avoid weak numerical instabilities from developing. The instability is eliminated if the waves that are unresolved by the outer nest are damped at outflow boundaries rather than being allowed to reflect. We compare WLPFK3 and WLAPK5 to assess the effects of two-way interaction.

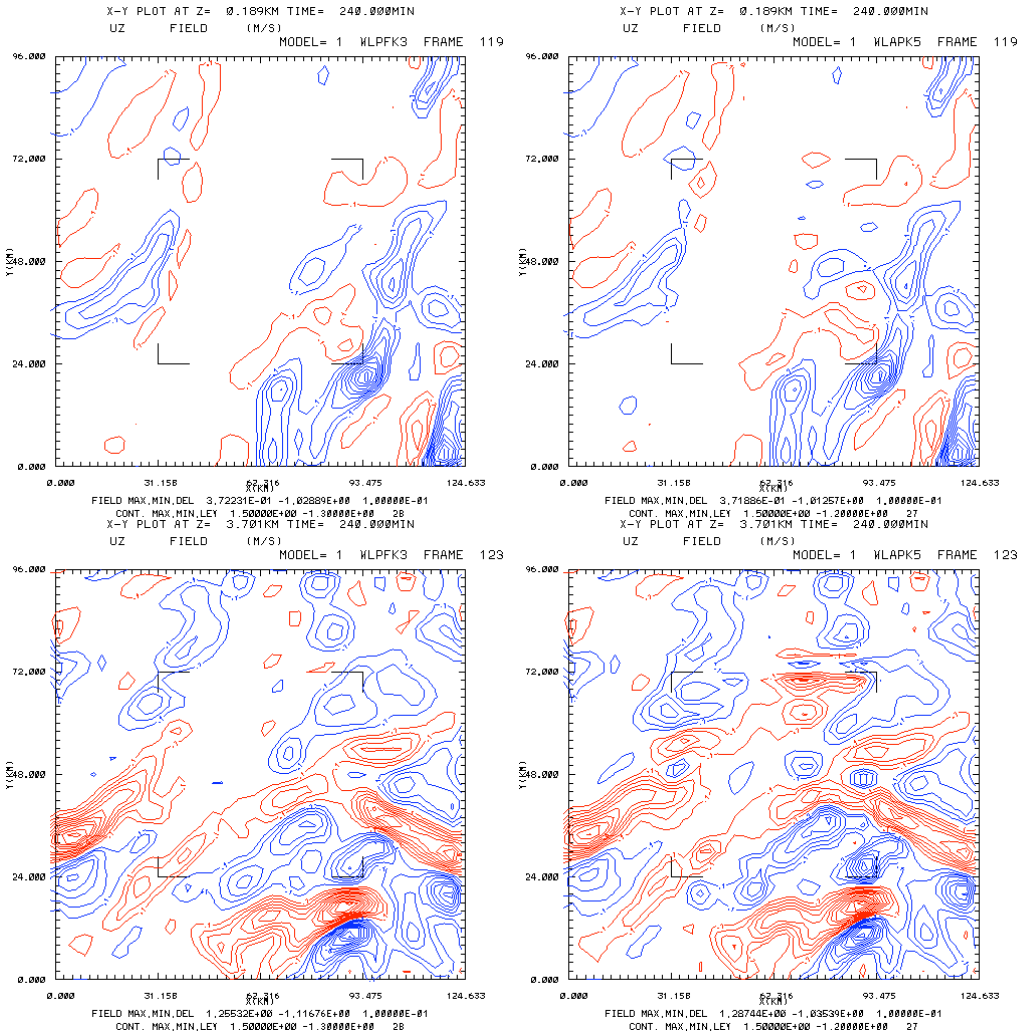

Figure 3-8. *w* at z = 0.189 and 3.70 km AGL for WLPFK3 (one-way) and WLAPK5(two-way) for outer layer (2 km grid).

Figures 3-8 and 3-9 show *w* at two height levels for both the outer (2 km grid) and inner (1 km grid) layers at t = 3 hrs into the forecast. There are some differences but mostly minor. *w* showed the most significant differences (although minor) and the u, v and θ fields (not shown) showed even less effect of the two-way interaction. These are encouraging results because we have not significantly changed the physics of the model. The only differences were in numerical treatments that one would expect to have a minor effect. The next section shows the effect of making the first major change to the physics, i.e. increasing the resolution of the topography.

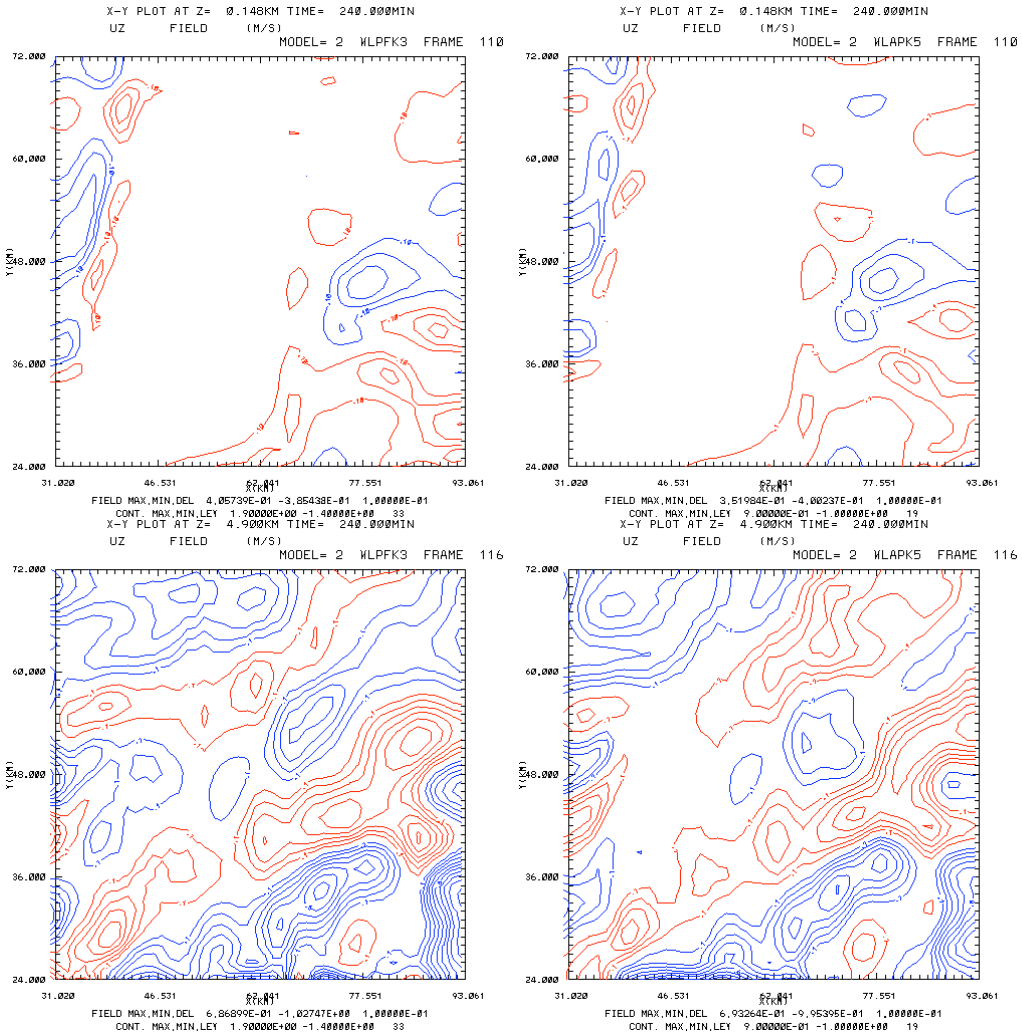

Figure 3-9. *w* at z = 0.189 and 3.70 km AGL for WLPFK3 (one-way) and WLAPK5(two-way) for inner layer (1 km grid).

g. Effect of Higher Resolution Orography

Figure 3-10 shows the difference between the higher resolution WFIS and the MC2 orography. The WFIS orography was derived using 30 arc second USGS data. The height of the topography at each grid point of the WFIS model was determined by integrating the area of the grid over the USGS data. To suppress high frequency modes a single application of a bi-directional 1-2-1 (9-point) filter was applied to the data. As we see in Fig. 3-10 the differences result in ± 250 m for layer-1 (2 km grids) and + 340 and -280 m for layer-2 (1 km grid). With these strong differences in topographic forcing we should expect some significant differences in both the data projection as well as the WFIS model predictions.

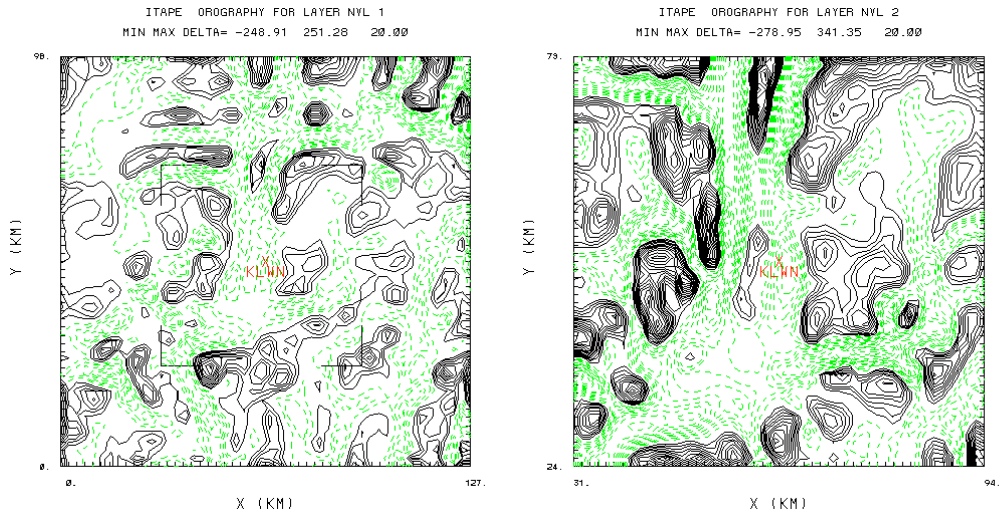

Figure 3-10. Difference between high resolution and MC2 interpolated orography. Contour interval is 20 m with black (green) representing positive (negative) differences.

Figure 3-11 shows a comparison between the w fields of MC2WL3 and MC2WL6 at two height levels z = 0.189 and 3.70 km AGL. We see a significant difference resulting from projecting the MC2 data onto a WFIS grid that uses a higher resolution topography than that which is consistent with the MC2 data. The high amplitude pattern of up- and downdrafts shown in Fig. 3-11 result from the added small scale structure to the topography as shown in Fig. 3-10. The effect of using the increased topographic resolution can be seen in Fig. 3-12 where w is shown for WLAPk5 and WLAPK6 at t = 3 hrs at z = .0189 and 3.70 km AGL. We see a significant increase in the horizontal variability of the w field as well as an increase in the amplitudes resulting from the increased topographic resolution.

The projected data from the MC2 is significantly modified from using higher resolution topography that is inconsistent with the MC2 data. This initialization means we can expect the WFIS model will need to adjust to the new forcing and if the boundary conditions are sufficiently accurate then the accuracy of the local forecasts should improve. Logically, the WFIS forecasts using higher resolution should be compared with the MC2 forecasts using the lower resolution MC2 topography.

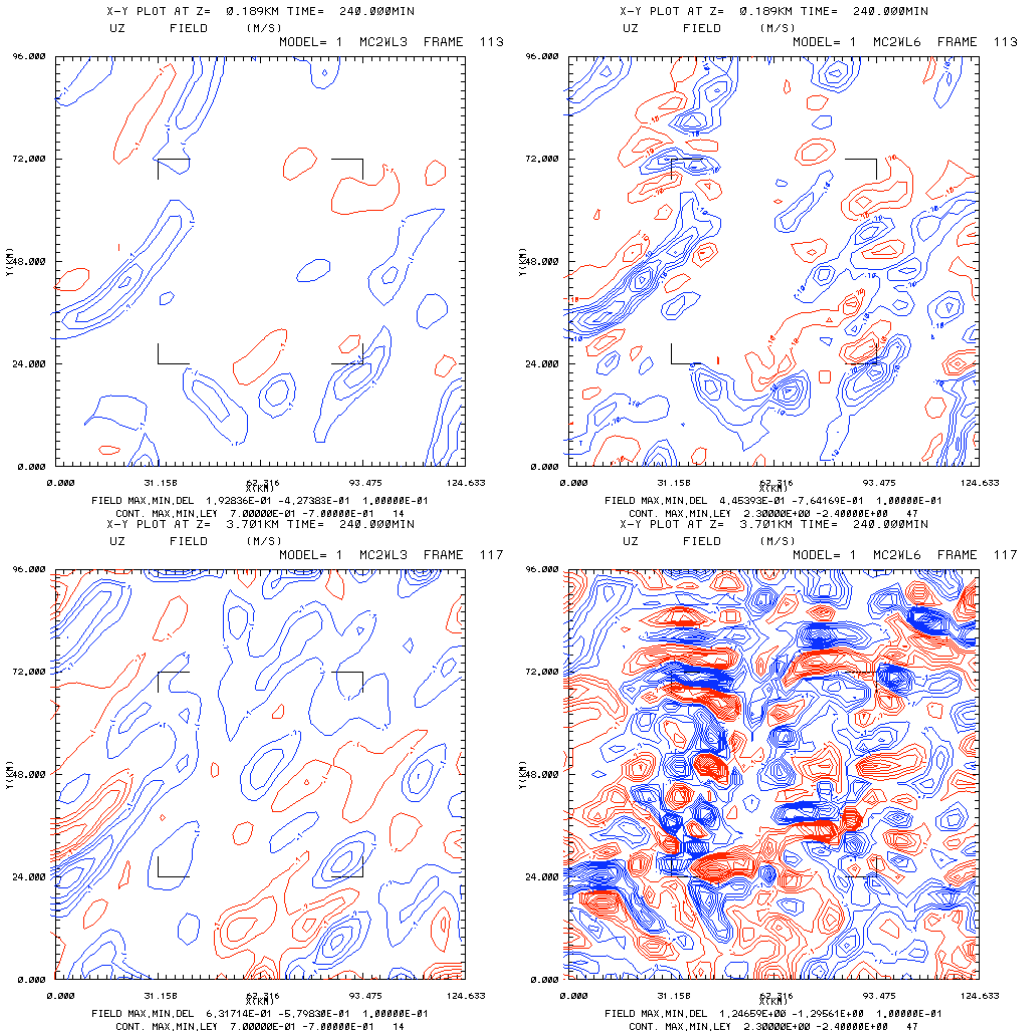

Figure 3-11. MC2LW3 and MC2LW6 w fields for z = 0.189 and 3.7 km AGL at t = 3 hrs (local noon)

Figure 3-12 shows a comparison between the 3 hr WFIS forecast using low-resolution topography (WLAPK5) and using high resolution topography (WLAPK6). The w field from WLAPK6 shows most of the same features seen in WLAPK5 but with the addition of finer scale features. The maximum amplitudes have also increased by about 30 %.

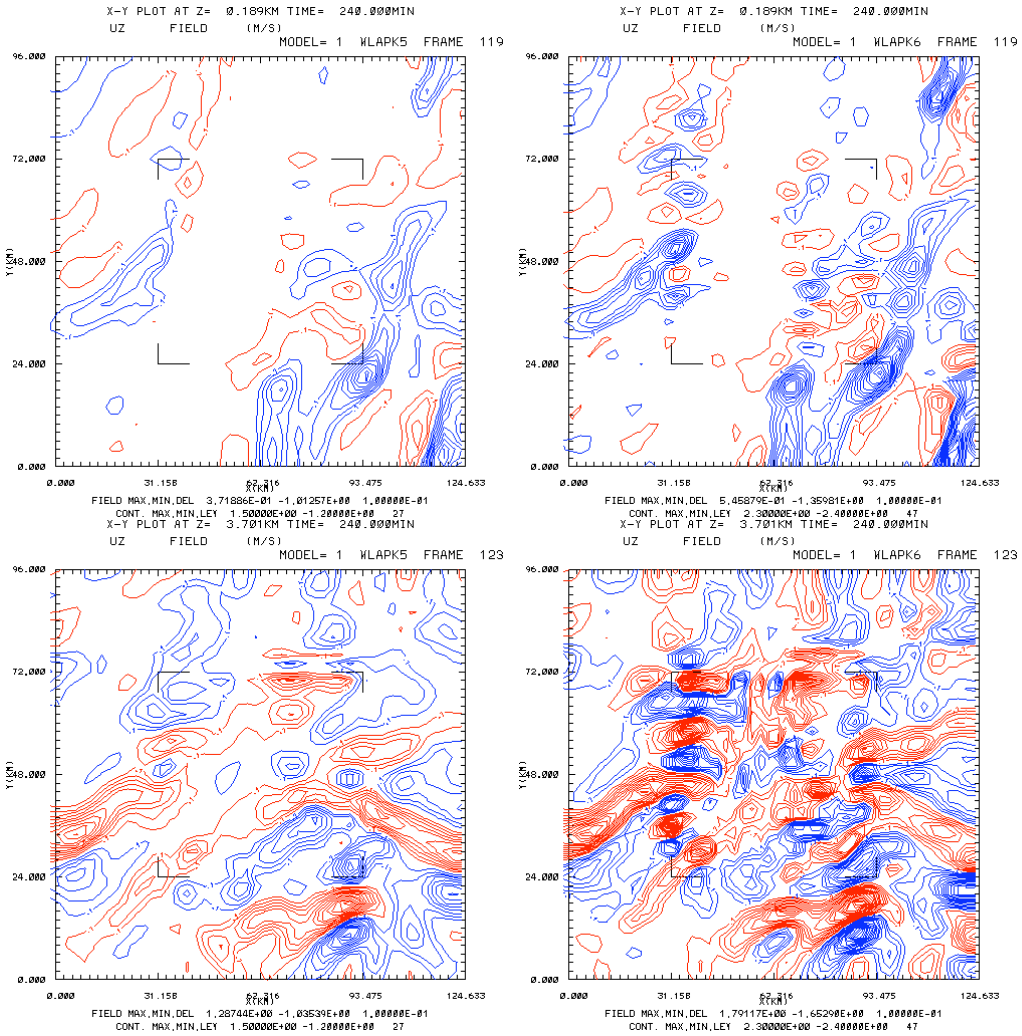

Figure 3-12. WLAPK5 and WLAPK6 comparisons of w for z = 0.189 and 3.7 km AGL at t= 3 hrs. Result shown are for the outer nest.

h. Comparison between Kelowna Sounding Data and Model Predictions

Experiments WLAPK5 and WLAPK6 were extended to 6 hrs (3 pm local) to allow for comparison between the model predictions and the Kelowna soundings. The MC2WL3 and MC2WL6 projected data as well as the WFIS data are compared.

Figure 3-13 shows a comparison between the MC2 and WFIS model forecasts for 3 pm (local) time at Kelowna. Only MC2WL6 data is shown because the projection of MC2WL3 was effectively identical. The top three plots show MC2WL6 predictions of u, v and temperature. The comparison between u and v show the presence of strong NE mid-troposphere winds in the MC2 forecast whereas the observations show WNW winds. The comparison suggests that the MC2 forecasted the position of a low pressure system too far to the west of Kelowna.

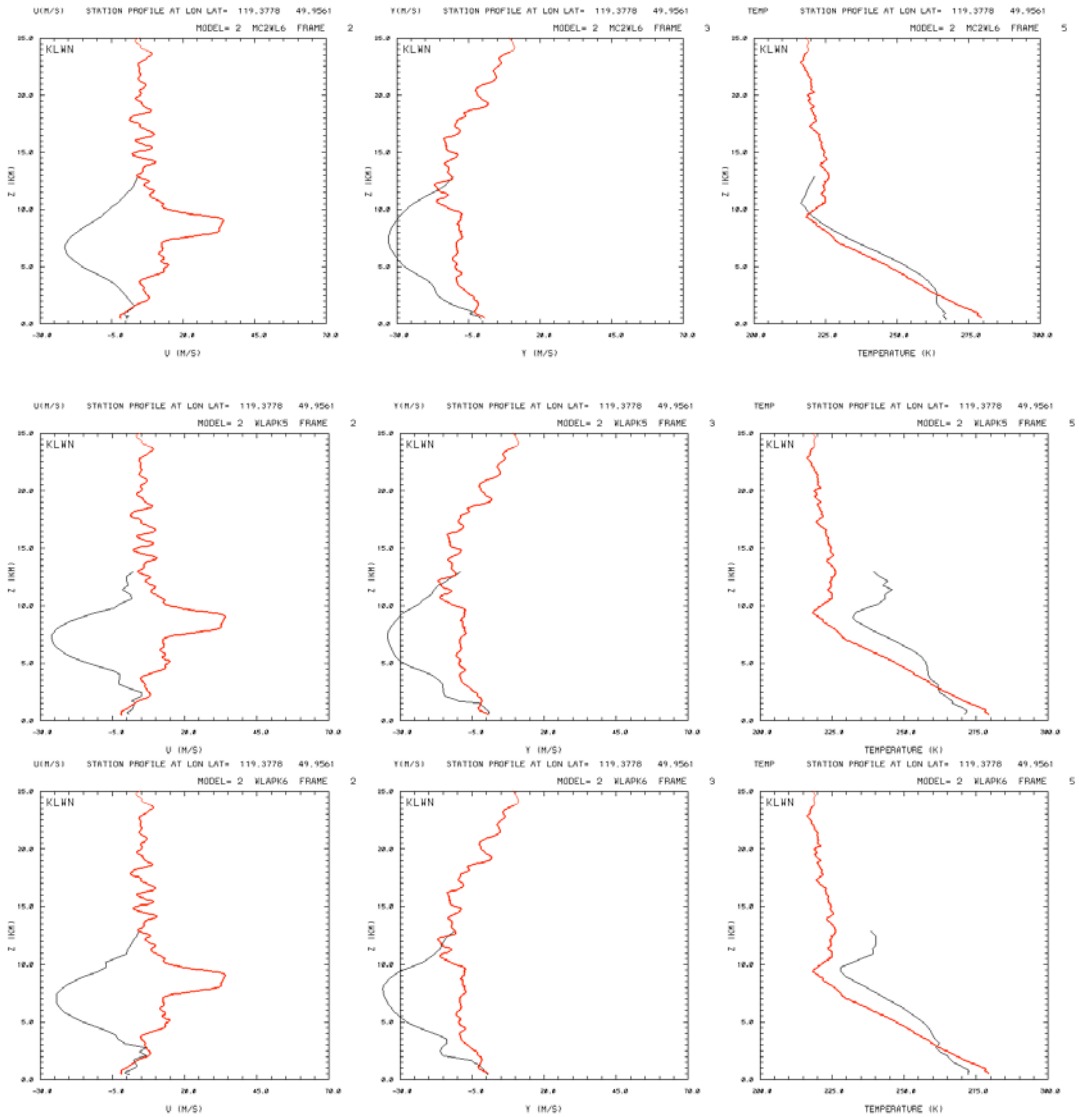

Figure 3-13. MC2WL6, WLAPK5 and WLAPK6 comparisons with the 3 pm Kelowna sounding data for the inner nest. Data shown is for u, v and temperature. The thin (black) line shows MC2 model data (top three plots) and WFIS model data (bottom 6 plots) whereas the thick (red) line shows the observations.

The near surface temperatures are also predicted about 12 C too cold. Since the WFIS model takes its initial and boundary conditions from the MC2 its forecasts show similar poor comparison. The only reasonable aspect of both the MC2 and WFIS forecasts is the near surface winds seem to agree with the observations. However, considering the other data this may simply be fortuitous.

It seems clear that one cannot draw many conclusions regarding the performance of the WFIS model from the above comparisons. A more in depth comparison of the large scale weather patterns between the observations and forecasts is required as well as cases where the MC2 has performed better than it has for this case.

i. Conclusions and Future Work

The limited funding of this aspect of the WLAP project did not allow sufficient time to go beyond what we have presented. The results to-date are encouraging. There are numerous aspects of the physics that could be considered with further funding.

Radiation and surface budgets

In the simulations presented the short and long wave radiation physics of the WFIS code were not active. The combination of the limited integration period (3 or 6 hours) combined with the small domain size limits the negative effects of not considering this physical forcing because one might argue that this effect is being supplied by the boundary conditions. However, one should really have the model accepting the boundary conditions (WFIS) be physically compatible with the larger scale model (MC2).

The increased resolution of the WFIS code could be explored in the area or physical response to solar heating. Shadowing effects would be particularly more pronounced as the resolution is increased. It would be interesting to explore the amplitude of such effects at periods near sunrise as well as sunset.

Higher Resolution

The resolution of the WFIS code was extended to only 1 km as again this is all that was possible in the short grant period. Much higher horizontal resolution could also be considered. The WFIS code is well suited for vertical grid refinement and the effects of increased resolution in the lowest levels could also be explored. It should be noted that RAMS does not posses this capability as pointed out by Clark and Hall (1996, JAM).

Treatments of topographic resolution changes

Further study is needed to assess how forecast accuracy might be achieved by locally increasing the resolution of the topographic and thermal forcing while using initial and boundary condition forcing from a lower resolution model. Proxy data might be one approach to consider for assessing simple procedures without getting into the complexities of four dimensional data assimilation. The premise of such research assumes that much of the local meteorology is locally caused.

4. Overall Recommendations: Ensemble Forecasts

UBC has a demonstrated capability to produce real-time high-resolution weather forecasts down to 2 km horizontal grid spacing using MC2, and to produce *ex-post-facto* weather simulations to grid spacings of 100s to 10s of meters using WFIS. In separate work not reported here, we have also just achieved 2 km grid spacing with the MM5 model for real-time weather forecasts. This allows ensemble forecasts (MC2, WFIS, & MM5) at 2 km grid spacing. Ensemble-average weather forecasts are more accurate than single categorical NWP forecasts, and provide a better meteorological driver for fine-resolution air quality models such as CMAQ and CALPUFF/CALGRID. Ensemble forecasts are a cutting-edge approach that can be utilized by WLAP.

Appendix A - Data File Information

Data provided for this project was primarily Vis5D files of MC2 output for the fourth (4km) and fifth (4km) grids. These files cover two case study periods (June 12-26, 2002 and January 28 -February 10, 2003) and the general forecast period from February 1, 2003 to March 31, 2003. For each day within these periods, the latter 45 hours of a sixty hour forecast was provided for each grid. Each hour comprised one Vis5D file. The files are named xxxxM where 'xxxx' is the offset of the forecast in minutes from initialization (ie 0Z). To readily identify the date each file is associated with, files are then stored in directories named YYMMDD00/d4.v5d and YYMMDD00/d5.v5d for the fourth (4km) and fifth (2km) grids respectively where YY is the last two digits of the year, MM is the month (01-12), and DD is the day (01-31) of the date for which the files were generated. An example file and directory would be 03020900/d4.v5d/1440M. Files are each about 16MB zipped and 37MB unzipped.

Additional output from Terry Clark's model for these case studies will be provided in GIF and JPG formats. Exact sizes are not known at the time of writing, however, it is anticipated that total file size will likely not exceed 1GB.

Finally MC2 output in FST/Gal Chen format for the case study periods was also provided. This data can serve as input to Terry Clark's model. These files were stored in directories named after the date (YYMMDD00) and have filenames following the protocol **YYMMDD00_Dkm.00xxxx.G** where 'YYMMDD00' follows the format outlined above for the Vis5D files, 'D' represents the grid size (either 2 or 4), and 'xxxx' follows the time offset as outlined above for the Vis5D files. An example directory and file would be 03022800/03022800_2km.001440.G. These files are approximately 80-90MB uncompressed, and only slightly smaller (70MB) compressed.

Appendix B. Verification Statistics

Kamloops area
Summary statistics for 2003-02-01 through 2003-03-31 inclusive
Model: MC2 run at 4.0 grid spacing
Number of stations used in analysis: 15

Air Temperatures (degrees C)

Forecast Time Range	Number of Data Pairs	Mean Error	Mean Absolute Error	RMSE	Error Variance	Correlation
1 - 11 hours	1091	-3.8	4.08	5.38	15	0.63
12 - 23 hours	4658	-4.28	4.5	5.79	15	0.77
24 - 35 hours	4405	-3.87	4.15	5.39	14	0.72
36 - 47 hours	4477	-3.99	4.53	5.79	18	0.73
48 - 59 hours	4176	-3.57	4.18	5.48	17	0.66
60 - 71 hours	349	-3.28	3.98	5.32	18	0.57

Forecast Time Range	Slope	Forecast Variance	Observation Variance
1 - 11 hours	0.42	11	24
12 - 23 hours	0.54	18	37
24 - 35 hours	0.52	15	29
36 - 47 hours	0.51	18	38
48 - 59 hours	0.46	15	31
60 - 71 hours	0.39	12	25

Surface Atmospheric Pressure (kPa)

Forecast Time Range	Number of Data Pairs	Mean Error	Mean Absolute Error	RMSE	Error Variance	Correlation
1 - 11 hours	162	-3.18	3.13	3.18	0	0.97
12 - 23 hours	601	-3.24	3.19	3.25	0	0.96
24 - 35 hours	638	-3.25	3.2	3.27	0	0.95
36 - 47 hours	570	-3.27	3.23	3.3	0	0.94
48 - 59 hours	604	-3.25	3.2	3.27	0	0.92
60 - 71 hours	51	-3.29	3.25	3.28	0	0.93

Forecast Time Range	Slope	Forecast Variance	Observation Variance
1 - 11 hours	0.97	1	1
12 - 23 hours	1.02	1	1
24 - 35 hours	1.09	1	1
36 - 47 hours	1.09	1	1
48 - 59 hours	1.1	1	1
60 - 71 hours	1.06	1	1

Hourly Precipitation (mm of water equivalent)

Forecast Time Range	Number of Data Pairs	Mean Error	Mean Absolute Error	RMSE	Error Variance	Correlation
1 - 11 hours	617	0	0.01	0.12	0	-9999
12 - 23 hours	2842	-0.04	0.05	0.41	0	-0.05
24 - 35 hours	2728	-0.02	0.02	0.19	0	-0.24
36 - 47 hours	2745	-0.04	0.05	0.42	0	-0.05
48 - 59 hours	2603	-0.01	0.03	0.24	0	-0.15
60 - 71 hours	209	0.01	0.01	0.12	0	-9999

Forecast Time Range	Slope	Forecast Variance	Observation Variance
1 - 11 hours	-9999	0	0
12 - 23 hours	-0.02	0	0
24 - 35 hours	-0.14	0	0
36 - 47 hours	-0.03	0	0
48 - 59 hours	-0.17	0	0
60 - 71 hours	-9999	0	0

Relative Humidity

Forecast Time Range	Number of Data Pairs	Mean Error	Mean Absolute Error	RMSE	Error Variance	Correlation
1 - 11 hours	589	0.25	11.56	15.04	226	0.22
12 - 23 hours	2798	2.84	13.87	18.24	325	0.5
24 - 35 hours	2673	2.86	13.43	18.03	317	0.42
36 - 47 hours	2727	3.69	14.02	18.53	330	0.51
48 - 59 hours	2570	4.08	14	18.91	341	0.4
60 - 71 hours	192	0.22	11.35	15.44	238	0.1

Forecast Time Range	Slope	Forecast Variance	Observation Variance
1 - 11 hours	0.12	66	212
12 - 23 hours	0.32	168	425
24 - 35 hours	0.25	126	373
36 - 47 hours	0.3	154	443
48 - 59 hours	0.22	119	393
60 - 71 hours	0.05	51	209

Wind Speed (km/hour)

Forecast Time Range	Number of Data Pairs	Mean Error	Mean Absolute Error	RMSE	Error Variance	Correlation
1 - 11 hours	1091	0.16	3.53	5.84	34	0.14
12 - 23 hours	4660	0.94	3.62	6.05	29	0.27
24 - 35 hours	4403	-1.68	3.09	5.19	24	0.27
36 - 47 hours	4479	-2.69	3.75	6.23	32	0.26
48 - 59 hours	4176	-1.6	3.18	5.24	25	0.25
60 - 71 hours	349	-1	3.01	5.08	25	0.23

Forecast Time Range	Slope	Forecast Variance	Observation Variance
1 - 11 hours	0.13	18	22
12 - 23 hours	0.09	4	32
24 - 35 hours	0.1	4	26
36 - 47 hours	0.09	4	34
48 - 59 hours	0.1	4	26
60 - 71 hours	0.09	4	25

Vector Wind U-Component (km/hour)

Forecast Time Range	Number of Data Pairs	Mean Error	Mean Absolute Error	RMSE	Error Variance	Correlation
1 - 11 hours	1091	0.88	2.82	4.87	23	0.25
12 - 23 hours	4660	-0.14	2.47	4.56	21	0.31
24 - 35 hours	4403	0.09	2.19	4	16	0.31
36 -47 hours	4479	-0.35	2.65	4.81	23	0.28
48 - 59 hours	4176	-0.06	2.33	4.17	17	0.26
60 - 71 hours	349	-0.08	2.17	4.02	16	0.23

Forecast Time Range	Slope	Forecast Variance	Observation Variance
1 - 11 hours	0.25	15	16
12 - 23 hours	0.13	4	23
24 - 35 hours	0.15	4	17
36 - 47 hours	0.12	4	24
48 - 59 hours	0.13	5	17
60 - 71 hours	0.12	4	15

Vector Wind V-Component (km/hour)

Forecast Time Range	Number of Data Pairs	Mean Error	Mean Absolute Error	RMSE	Error Variance	Correlation
1 - 11 hours	1091	0.4	2.63	4.67	22	0.33
12 - 23 hours	4660	-0.34	2.72	4.87	24	0.42
24 - 35 hours	4403	0.05	2.53	4.43	20	0.39
36 - 47 hours	4479	-0.11	2.91	5.09	26	0.42
48 - 59 hours	4176	0.26	2.62	4.52	20	0.39
60 - 71 hours	349	0.57	2.3	4.27	18	0.39

Forecast Time Range	Slope	Forecast Variance	Observation Variance
1 - 11 hours	0.32	16	17
12 - 23 hours	0.17	5	29
24 - 35 hours	0.2	6	23
36 - 47 hours	0.18	6	31
48 - 59 hours	0.2	6	24
60 - 71 hours	0.21	6	21

Mean Sea Level Pressure (kPa)

Forecast Time Range	Number of Data Pairs	Mean Error	Mean Absolute Error	RMSE	Error Variance	Correlation
1 - 11 hours	190	0.22	0.27	0.37	0	0.97
12 - 23 hours	619	0.11	0.25	0.36	0	0.96
24 - 35 hours	710	0.03	0.27	0.41	0	0.96
36 - 47 hours	592	0.03	0.35	0.49	0	0.94
48 - 59 hours	683	0.01	0.41	0.56	0	0.91
60 - 71 hours	52	0.12	0.4	0.53	0	0.92

Forecast Time Range	Slope	Forecast Variance	Observation Variance
1 - 11 hours	1.04	1	1
12 - 23 hours	1.1	1	1
24 - 35 hours	1.19	2	1
36 - 47 hours	1.18	2	1
48 - 59 hours	1.17	2	1
60 - 71 hours	1.16	2	1

Kelowna area
Summary statistics for 2003-02-01 through 2003-03-31 inclusive
Model: MC2 run at 4.0 grid spacing
Number of stations used in analysis: 13

Air Temperatures (degrees C)

Forecast Time Range	Number of Data Pairs	Mean Error	Mean Absolute Error	RMSE	Error Variance	Correlation
1 - 11 hours	930	-4.92	5.37	6.6	19	0.65
12 - 23 hours	3585	-5.36	5.46	6.59	15	0.78
24 - 35 hours	3574	-4.95	5.17	6.35	16	0.72
36 - 47 hours	3398	-5.1	5.48	6.6	18	0.74
48 - 59 hours	3367	-4.73	5.32	6.49	20	0.65
60 - 71 hours	291	-4.69	5.55	6.74	23	0.56

Forecast Time Range	Slope	Forecast Variance	Observation Variance
1 - 11 hours	0.36	10	33
12 - 23 hours	0.55	18	37
24 - 35 hours	0.48	14	33
36 - 47 hours	0.51	18	38
48 - 59 hours	0.42	15	34
60 - 71 hours	0.32	11	34

Surface Atmospheric Pressure (kPa)

Forecast Time Range	Number of Data Pairs	Mean Error	Mean Absolute Error	RMSE	Error Variance	Correlation
1 - 11 hours	306	1.3	3.45	3.81	13	0.22
12 - 23 hours	1073	1.01	3.35	3.7	13	0.24
24 - 35 hours	1152	1.05	3.37	3.72	13	0.21
36 - 47 hours	1017	0.98	3.35	3.7	13	0.24
48 - 59 hours	1085	1.04	3.36	3.72	13	0.2
60 - 71 hours	93	1.13	3.42	3.77	13	0.24

Forecast Time Range	Slope	Forecast Variance	Observation Variance
1 - 11 hours	0.05	1	13
12 - 23 hours	0.06	1	13
24 - 35 hours	0.06	1	13
36 - 47 hours	0.07	1	13
48 - 59 hours	0.06	1	13
60 - 71 hours	0.07	1	14

Hourly Precipitation (mm of water equivalent)

Forecast Time Range	Number of Data Pairs	Mean Error	Mean Absolute Error	RMSE	Error Variance	Correlation
1 - 11 hours	303	-0.06	0.05	0.26	0	-9999
12 - 23 hours	1250	-0.07	0.06	0.34	0	-0.13
24 - 35 hours	1282	-0.06	0.06	0.28	0	-0.6
36 - 47 hours	1178	-0.08	0.06	0.34	0	-9999
48 - 59 hours	1221	-0.06	0.07	0.31	0	-0.31
60 - 71 hours	96	-0.08	0.05	0.24	0	-9999

Forecast Time Range	Slope	Forecast Variance	Observation Variance
1 - 11 hours	-9999	0	0
12 - 23 hours	-0.05	0	0
24 - 35 hours	-0.09	0	0
36 - 47 hours	-9999	0	0
48 - 59 hours	-0.1	0	0
60 - 71 hours	-9999	0	0

Relative Humidity

Forecast Time Range	Number of Data Pairs	Mean Error	Mean Absolute Error	RMSE	Error Variance	Correlation
1 - 11 hours	267	10.76	15.09	19.76	275	0.19
12 - 23 hours	1194	11.94	15.51	19.62	242	0.57
24 - 35 hours	1214	13.25	16.54	21.68	295	0.43
36 - 47 hours	1152	11.95	15.87	20.13	263	0.52
48 - 59 hours	1161	13.45	16.98	22.17	311	0.41
60 - 71 hours	85	8.73	13.5	17.98	248	0.23

Forecast Time Range	Slope	Forecast Variance	Observation Variance
1 - 11 hours	0.07	40	275
12 - 23 hours	0.31	107	360
24 - 35 hours	0.2	82	358
36 - 47 hours	0.29	107	362
48 - 59 hours	0.21	93	372
60 - 71 hours	0.09	40	255

Wind Speed (km/hour)

Forecast Time Range	Number of Data Pairs	Mean Error	Mean Absolute Error	RMSE	Error Variance	Correlation
1 - 11 hours	891	-2.16	3.99	6.17	33	0.04
12 - 23 hours	3419	-3.42	3.88	6.08	25	0.29
24 - 35 hours	3415	-3.07	3.89	6.12	28	0.18
36 - 47 hours	3244	-3.46	4	6.17	26	0.27
48 - 59 hours	3214	-3.08	3.94	6.17	29	0.18
60 - 71 hours	281	-2.65	3.66	5.84	27	0.11

Forecast Time Range	Slope	Forecast Variance	Observation Variance
1 - 11 hours	0.02	6	28
12 - 23 hours	0.08	2	27
24 - 35 hours	0.05	2	29
36 - 47 hours	0.08	3	28
48 - 59 hours	0.05	2	29
60 - 71 hours	0.03	2	27

Vector Wind U-Component (km/hour)

Forecast Time Range	Number of Data Pairs	Mean Error	Mean Absolute Error	RMSE	Error Variance	Correlation
1 - 11 hours	891	-0.45	3.69	5.77	33	0.02
12 - 23 hours	3419	-0.44	2.96	4.84	23	0.13
24 - 35 hours	3415	-0.72	3.21	5.22	27	0
36 - 47 hours	3244	-0.48	3.07	4.94	24	0.14
48 - 59 hours	3214	-0.64	3.3	5.34	28	-0.01
60 - 71 hours	281	-1.13	3.04	4.98	24	0.03

Forecast Time Range	Slope	Forecast Variance	Observation Variance
1 - 11 hours	0.01	7	26
12 - 23 hours	0.05	3	23
24 - 35 hours	0	3	24
36 - 47 hours	0.05	3	23
48 - 59 hours	-0.01	3	25
60 - 71 hours	0.01	3	21

Vector Wind V-Component (km/hour)

Forecast Time Range	Number of Data Pairs	Mean Error	Mean Absolute Error	RMSE	Error Variance	Correlation
1 - 11 hours	891	1.55	3.61	5.97	33	0.17
12 - 23 hours	3419	0.14	3.24	5.42	29	0.35
24 - 35 hours	3415	1.32	3.43	5.68	31	0.3
36 - 47 hours	3244	0.48	3.49	5.73	33	0.29
48 - 59 hours	3214	1.44	3.69	5.99	34	0.24
60 - 71 hours	281	1.67	3.36	5.61	29	0.28

Forecast Time Range	Slope	Forecast Variance	Observation Variance
1 - 11 hours	0.1	9	30
12 - 23 hours	0.13	5	33
24 - 35 hours	0.11	4	34
36 - 47 hours	0.11	5	35
48 - 59 hours	0.09	5	35
60 - 71 hours	0.09	3	31

Mean Sea Level Pressure (kPa)

Forecast Time Range	Number of Data Pairs	Mean Error	Mean Absolute Error	RMSE	Error Variance	Correlation
1 - 11 hours	266	0.39	0.4	0.48	0	0.96
12 - 23 hours	887	0.33	0.36	0.47	0	0.95
24 - 35 hours	1023	0.27	0.36	0.48	0	0.95
36 - 47 hours	834	0.29	0.4	0.53	0	0.94
48 - 59 hours	963	0.3	0.46	0.61	0	0.9
60 - 71 hours	78	0.39	0.49	0.63	0	0.93

Forecast Time Range	Slope	Forecast Variance	Observation Variance
1 - 11 hours	1.06	1	1
12 - 23 hours	1.08	1	1
24 - 35 hours	1.19	1	1
36 - 47 hours	1.2	1	1
48 - 59 hours	1.19	1	1
60 - 71 hours	1.19	1	1

Kamloops area
Summary statistics for 2003-02-01 through 2003-03-31 inclusive
Model: MC2 run at 2.0 grid spacing
Number of stations used in analysis: 15

Air Temperatures (degrees C)

Forecast Time Range	Number of Data Pairs	Mean Error	Mean Absolute Error	RMSE	Error Variance	Correlation
12 - 23 hours	4550	-4.5	4.68	6.03	16	0.76
24 - 35 hours	4243	-4.15	4.35	5.61	14	0.72
36 - 47 hours	1432	-3.44	3.91	5.08	14	0.69

Forecast Time Range	Slope	Forecast Variance	Observation Variance
12 - 23 hours	0.53	18	38
24 - 35 hours	0.51	15	30
36 - 47 hours	0.45	12	27

Surface Atmospheric Pressure (kPa)

Forecast Time Range	Number of Data Pairs	Mean Error	Mean Absolute Error	RMSE	Error Variance	Correlation
12 - 23 hours	585	-2.88	2.83	2.9	0	0.95
24 - 35 hours	615	-2.89	2.84	2.91	0	0.95
36 - 47 hours	201	-2.91	2.86	2.92	0	0.95

Forecast Time Range	Slope	Forecast Variance	Observation Variance
12 - 23 hours	1.05	1	1
24 - 35 hours	1.12	1	1
36 - 47 hours	1.1	1	1

Hourly Precipitation (mm of water equivalent)

Forecast Time Range	Number of Data Pairs	Mean Error	Mean Absolute Error	RMSE	Error Variance	Correlation
12 - 23 hours	2785	-0.04	0.04	0.39	0	-0.04
24 - 35 hours	2625	-0.02	0.02	0.18	0	-0.29
36 - 47 hours	865	0	0.01	0.11	0	-9999

Forecast Time Range	Slope	Forecast Variance	Observation Variance
12 - 23 hours	-0.01	0	0
24 - 35 hours	-0.13	0	0
36 - 47 hours	-9999	0	0

Relative Humidity

Forecast Time Range	Number of Data Pairs	Mean Error	Mean Absolute Error	RMSE	Error Variance	Correlation
12 - 23 hours	2745	3.81	14.38	19.15	352	0.45
24 - 35 hours	2580	4.25	13.98	19.01	343	0.36
36 - 47 hours	809	-0.88	10.4	14.2	201	0.27

Forecast Time Range	Slope	Forecast Variance	Observation Variance
Initialization time	-9999	-9999	-9999
1 - 11 hours	-9999	-9999	-9999
12 - 23 hours	0.27	157	429
24 - 35 hours	0.2	116	380
36 - 47 hours	0.15	60	200
48 - 59 hours	-9999	-9999	-9999
60 - 71 hours	-9999	-9999	-9999
72 or more hours	-9999	-9999	-9999

Wind Speed (km/hour)

Forecast Time Range	Number of Data Pairs	Mean Error	Mean Absolute Error	RMSE	Error Variance	Correlation
12 - 23 hours	4552	-2.98	3.7	6.28	31	0.24
24 - 35 hours	4243	-2.23	3.06	5.37	24	0.27
36 - 47 hours	1432	-1.79	2.81	5.1	23	0.3

Forecast Time Range	Slope	Forecast Variance	Observation Variance
12 - 23 hours	0.08	4	32
24 - 35 hours	0.08	2	26
36 - 47 hours	0.09	2	25

Vector Wind U-Component (km/hour)

Forecast Time Range	Number of Data Pairs	Mean Error	Mean Absolute Error	RMSE	Error Variance	Correlation
12 - 23 hours	4552	-0.37	2.41	4.6	21	0.3
24 - 35 hours	4243	-0.39	2.07	3.98	16	0.3
36 - 47 hours	1432	-0.45	1.95	4	16	0.3

Forecast Time Range	Slope	Forecast Variance	Observation Variance
12 - 23 hours	0.11	3	23
24 - 35 hours	0.12	3	17
36 - 47 hours	0.11	2	17

Vector Wind V-Component (km/hour)

Forecast Time Range	Number of Data Pairs	Mean Error	Mean Absolute Error	RMSE	Error Variance	Correlation
12 - 23 hours	4552	-0.44	2.68	4.95	24	0.41
24 - 35 hours	4243	-0.04	2.37	4.43	20	0.39
36 - 47 hours	1432	0.39	2.05	3.98	16	0.45

Forecast Time Range	Slope	Forecast Variance	Observation Variance
12 - 23 hours	0.16	5	29
24 - 35 hours	0.16	4	23
36 - 47 hours	0.19	4	20

Mean Sea Level Pressure (kPa)

Forecast Time Range	Number of Data Pairs	Mean Error	Mean Absolute Error	RMSE	Error Variance	Correlation
12 - 23 hours	607	0.1	0.25	0.36	0	0.96
24 - 35 hours	676	0.06	0.28	0.42	0	0.96
36 - 47 hours	221	0.12	0.31	0.44	0	0.96

Forecast Time Range	Slope	Forecast Variance	Observation Variance
12 - 23 hours	1.11	1	1
24 - 35 hours	1.2	2	1
36 - 47 hours	1.16	2	1

Kelowna area
Summary statistics for 2003-02-01 through 2003-03-31 inclusive
Model: MC2 run at 2.0 grid spacing
Number of stations used in analysis: 13

Air Temperatures (degrees C)

Forecast Time Range	Number of Data Pairs	Mean Error	Mean Absolute Error	RMSE	Error Variance	Correlation
12 - 23 hours	3487	-6.09	6.16	7.37	17	0.74
24 - 35 hours	3448	-5.48	5.68	6.93	18	0.68
36 - 47 hours	1148	-4.73	5.39	6.64	22	0.66

Forecast Time Range	Slope	Forecast Variance	Observation Variance
12 - 23 hours	0.48	15	38
24 - 35 hours	0.42	13	33
36 - 47 hours	0.35	11	37

Surface Atmospheri Pressure (kPa)

Forecast Time Range	Number of Data Pairs	Mean Error	Mean Absolute Error	RMSE	Error Variance	Correlation
12 - 23 hours	1041	2.79	3.14	4.53	13	0.22
24 - 35 hours	1110	2.83	3.21	4.56	13	0.2
36 - 47 hours	369	2.93	3.28	4.64	13	0.25

Forecast Time Range	Slope	Forecast Variance	Observation Variance
12 - 23 hours	0.07	1	13
24 - 35 hours	0.06	1	13
36 - 47 hours	0.08	1	14

Hourly Precipitation (mm of water equivalent)

Forecast Time Range	Number of Data Pairs	Mean Error	Mean Absolute Error	RMSE	Error Variance	Correlation
12 - 23 hours	1213	-0.07	0.06	0.34	0	-0.13
24 - 35 hours	1241	-0.06	0.05	0.26	0	-9999
36 - 47 hours	393	-0.07	0.05	0.24	0	-9999

Forecast Time Range	Slope	Forecast Variance	Observation Variance
12 - 23 hours	-0.05	0	0
24 - 35 hours	-9999	0	0
36 - 47 hours	-9999	0	0

Relative Humidity

Forecast Time Range	Number of Data Pairs	Mean Error	Mean Absolute Error	RMSE	Error Variance	Correlation
12 - 23 hours	1178	18.15	20.37	25.82	337	0.29
24 - 35 hours	1181	17.57	20.02	26	368	0.15
36 - 47 hours	356	10.92	13.77	18.65	229	0.24

Forecast Time Range	Slope	Forecast Variance	Observation Variance
12 - 23 hours	0.12	64	363
24 - 35 hours	0.06	48	360
36 - 47 hours	0.07	22	241

Wind Speed (km/hour)

Forecast Time Range	Number of Data Pairs	Mean Error	Mean Absolute Error	RMSE	Error Variance	Correlation
12 - 23 hours	3332	-4.08	4.32	6.6	27	0.19
24 - 35 hours	3295	-3.75	4.21	6.42	27	0.13
36 - 47 hours	1098	-3.58	4.04	6.16	25	0.08

Forecast Time Range	Slope	Forecast Variance	Observation Variance
12 - 23 hours	0.05	2	28
24 - 35 hours	0.03	2	27
36 - 47 hours	0.02	1	25

Vector Wind U-Component (km/hour)

Forecast Time Range	Number of Data Pairs	Mean Error	Mean Absolute Error	RMSE	Error Variance	Correlation
12 - 23 hours	3332	-0.74	2.84	4.79	22	0.18
24 - 35 hours	3295	-1.02	2.99	4.95	23	0.17
36 - 47 hours	1098	-0.91	2.87	4.83	23	0.25

Forecast Time Range	Slope	Forecast Variance	Observation Variance
12 - 23 hours	0.05	2	23
24 - 35 hours	0.04	1	24
36 - 47 hours	0.06	1	24

Vector Wind V-Component (km/hour)

Forecast Time Range	Number of Data Pairs	Mean Error	Mean Absolute Error	RMSE	Error Variance	Correlation
12 - 23 hours	3332	-0.1	3.25	5.62	32	0.26
24 - 35 hours	3295	0.96	3.25	5.53	30	0.24
36 - 47 hours	1098	1.33	3.03	5.25	26	0.22

Forecast Time Range	Slope	Forecast Variance	Observation Variance
12 - 23 hours	0.08	3	34
24 - 35 hours	0.07	2	31
36 - 47 hours	0.06	2	27

Mean Sea Level Pressure (kPa)

Forecast Time Range	Number of Data Pairs	Mean Error	Mean Absolute Error	RMSE	Error Variance	Correlation
12 - 23 hours	867	0.39	0.41	0.51	0	0.95
24 - 35 hours	981	0.33	0.4	0.51	0	0.95
36 - 47 hours	310	0.39	0.44	0.55	0	0.96

Forecast Time Range	Slope	Forecast Variance	Observation Variance
12 - 23 hours	1.09	1	1
24 - 35 hours	1.18	1	1
36 - 47 hours	1.17	2	1

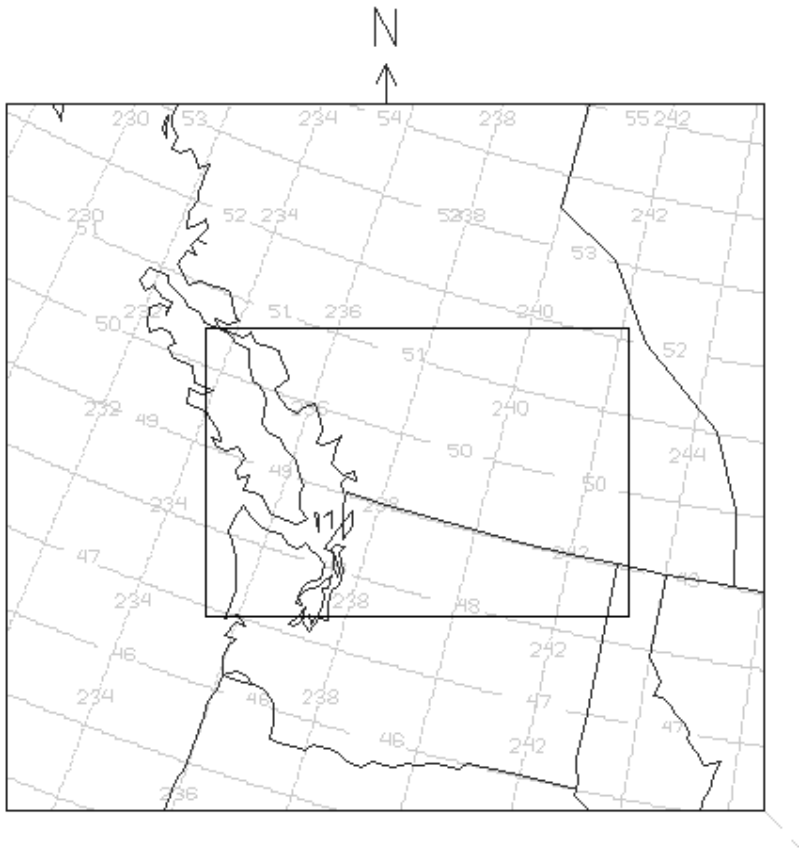

Fig 1.1 MC2 4 km domain with the 2 km domain placed within.

a) b)

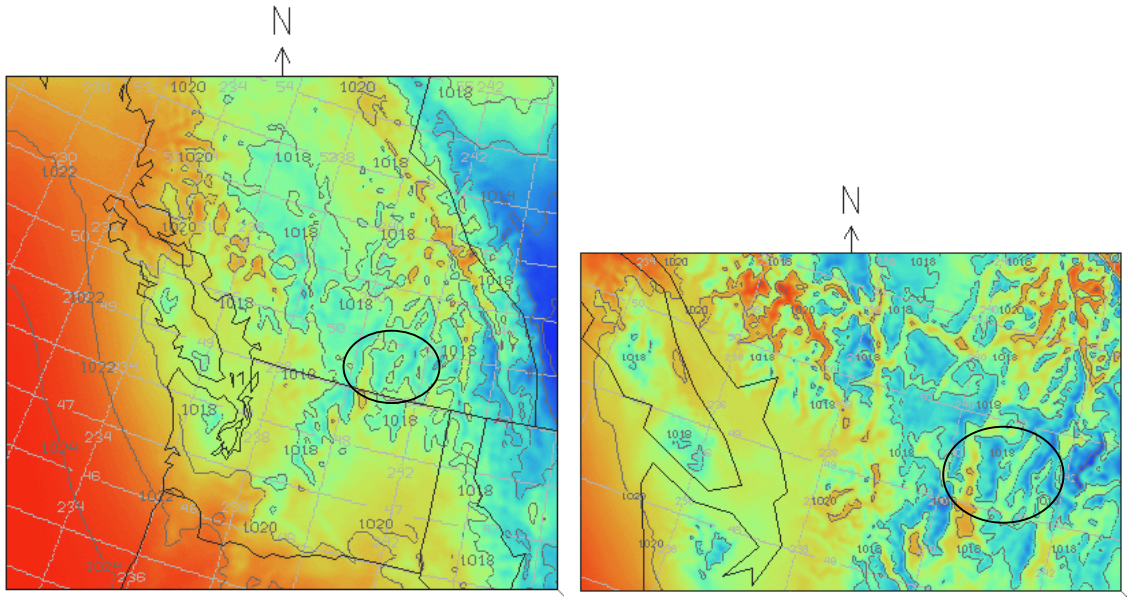

Fig 1.2 a & b Mean seal level pressure plots for the 4 km (a) and 2 km (b) MC2 grid output. Plots shown are of the 24 hour forecast from the 00Z February 1, 2003 initialization.

a b

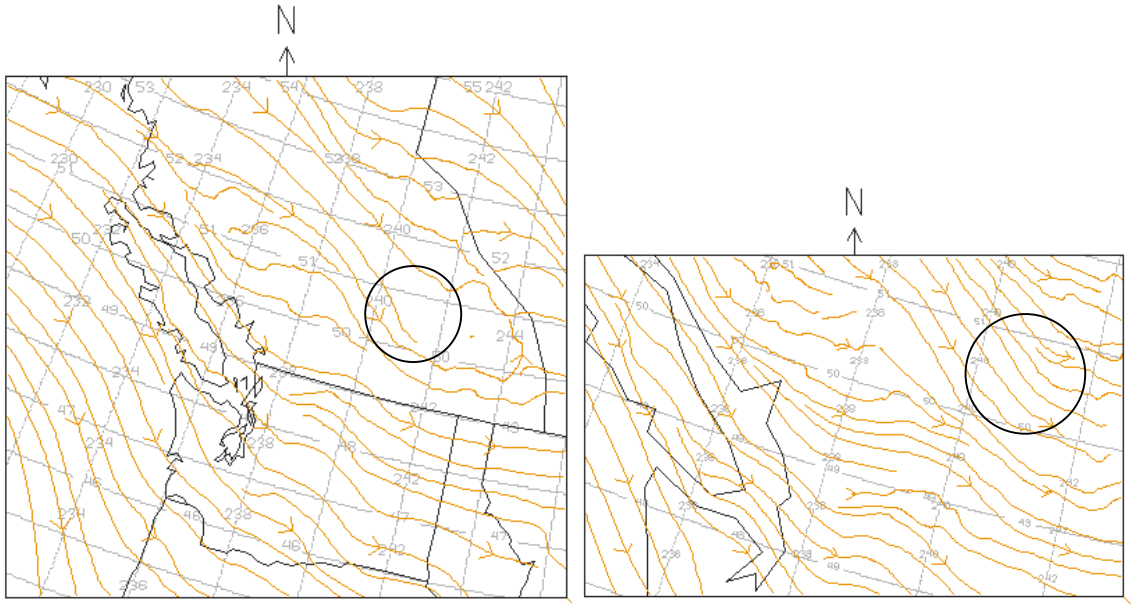

Fig. 1.3 a& b Streamlines of horizontal winds, at 82.4 kPa, for the 4 km (a) and 2 km (b) MC2 grid output. Images shown are from the 24 hr forecast of the initialization at 00Z February 1, 2003.

a) b)

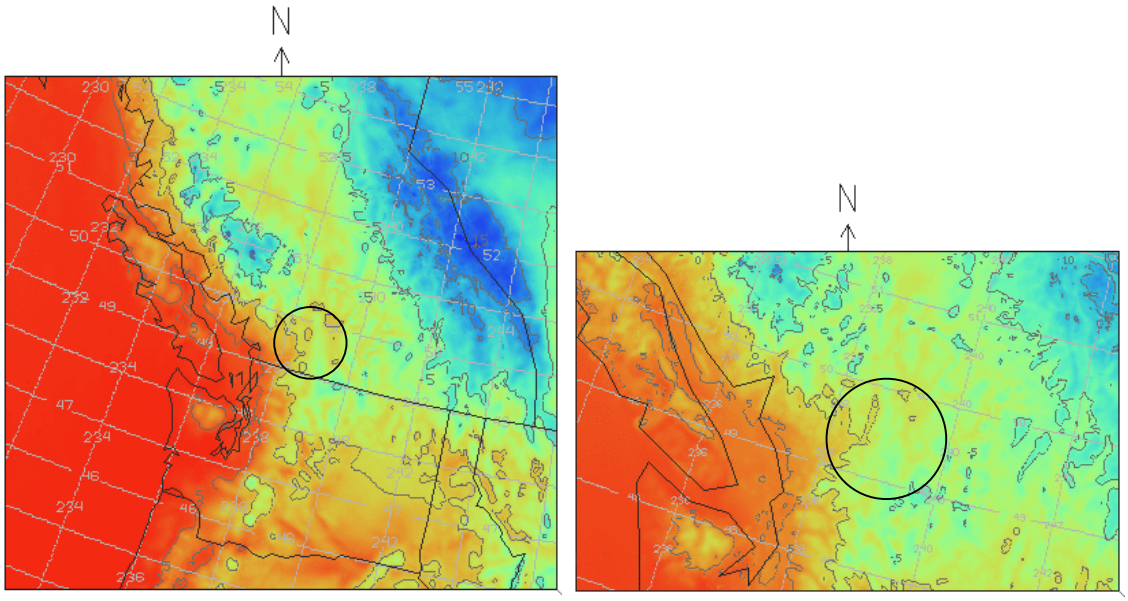

Fig. 1.4 a & b Surface temperature plots for the 4 km (a) and 2 km (b) MC2 grid spacing. Plots are from the 24 hour forecast of the 00Z February 1, 2003 model initialization.

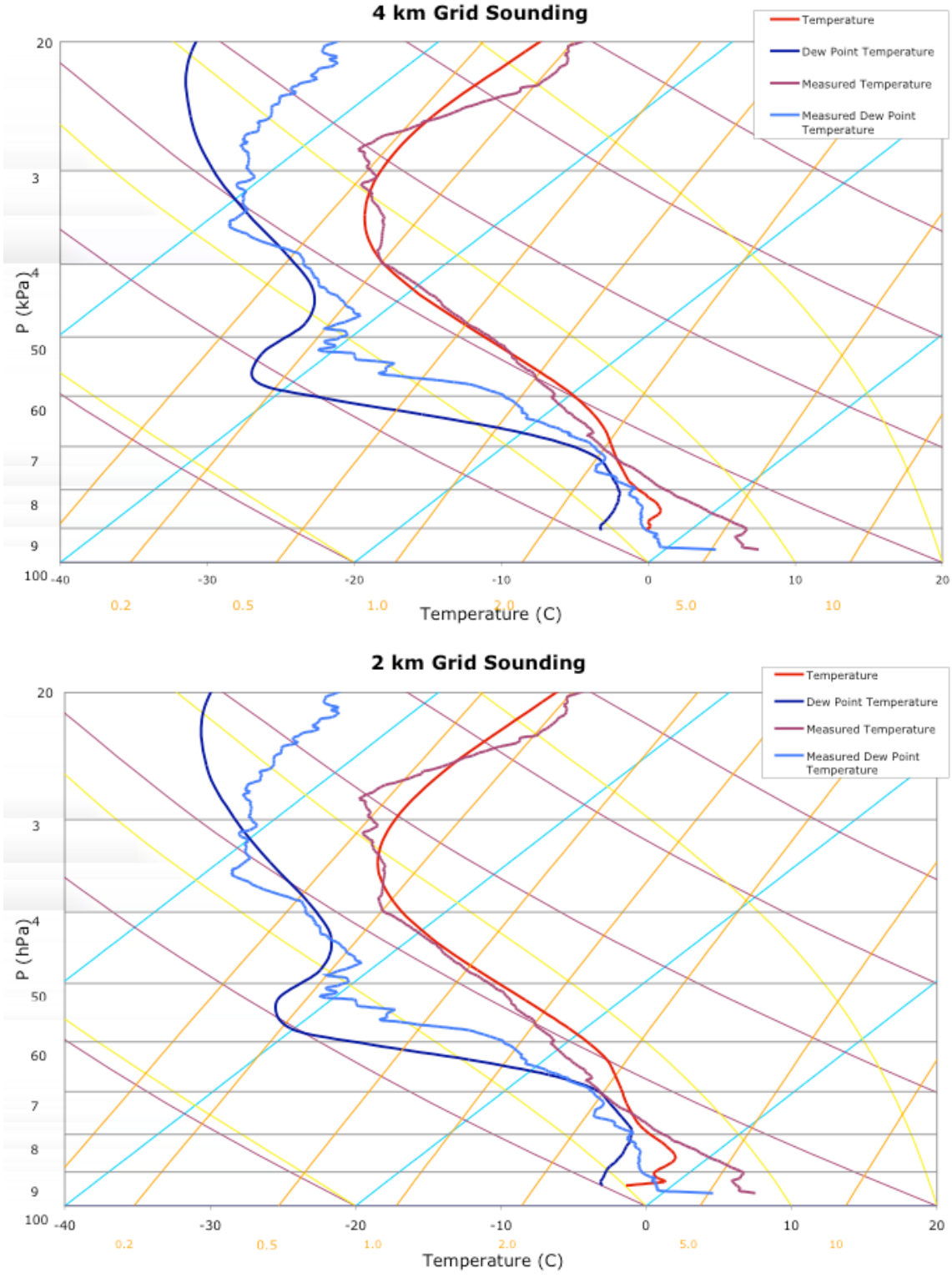

Fig. 1.5 a & b Forecast soundings produced by the 4 km grid and 2 km grid for Kelwona (49.93 N, 119.40 W, and, 456 m/MSL) from the 24 hour forecast of runs initialized at 00Z 1 February 2003, as well as the actual temperature and dew point temperature.

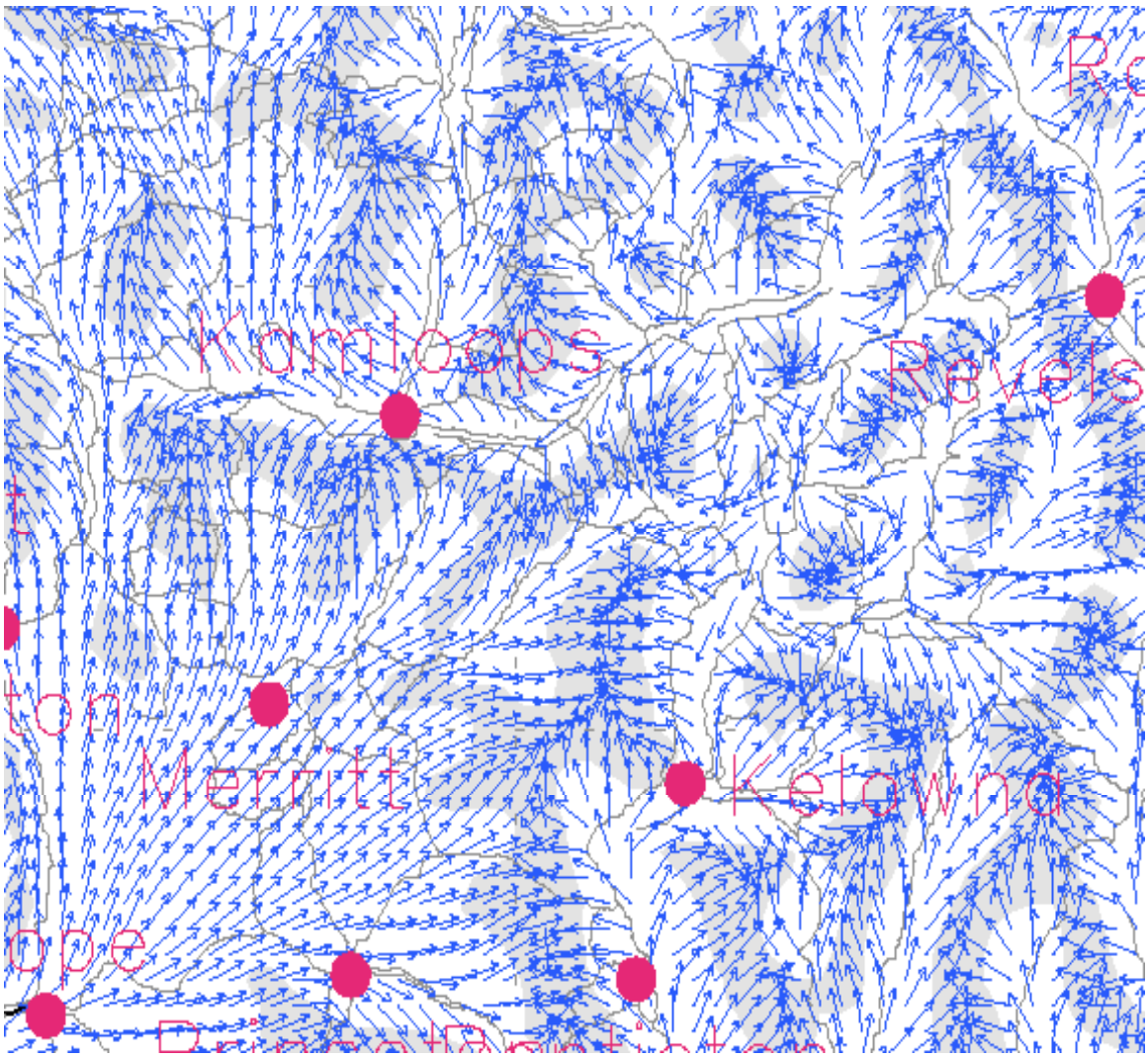

Fig. 1.6a. Surface winds and convergence for the 24 hour forecast produced by the 4 km grid of MC2, initialized 15 June 2002. Shaded areas indicate convergence. For comparison with the finer grid, note that Kamloops and Kelowna are the two red dots closest to the center of this domain.

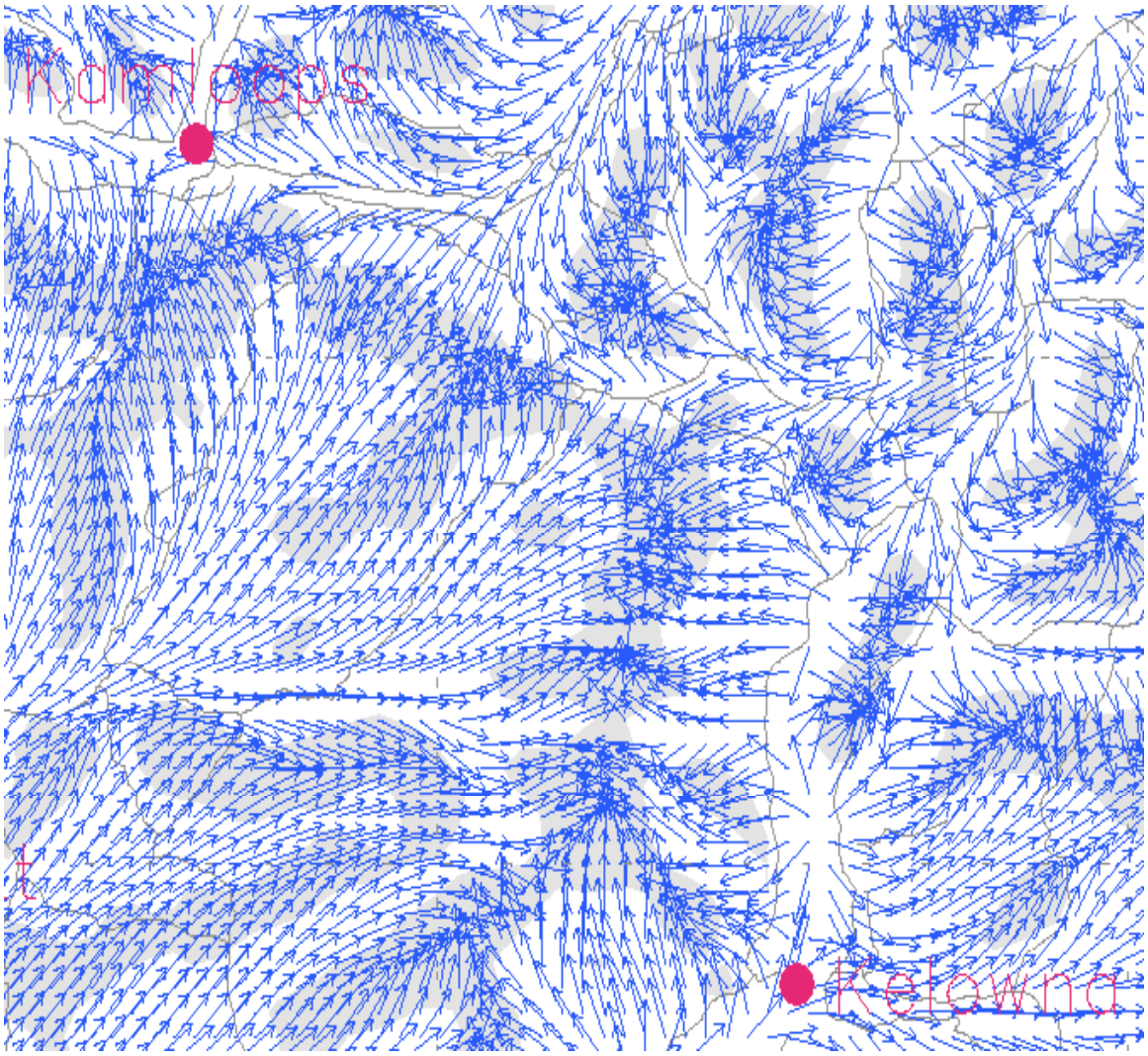

Fig. 1.6b. Surface winds and convergence from 24 hour forecast of 2 km grid, initialized at 00Z 15 June 2002. Shaded areas indicate regions of convergence. The upper left red dot is at Kamloops, and the lower right dot is at Kelowna.

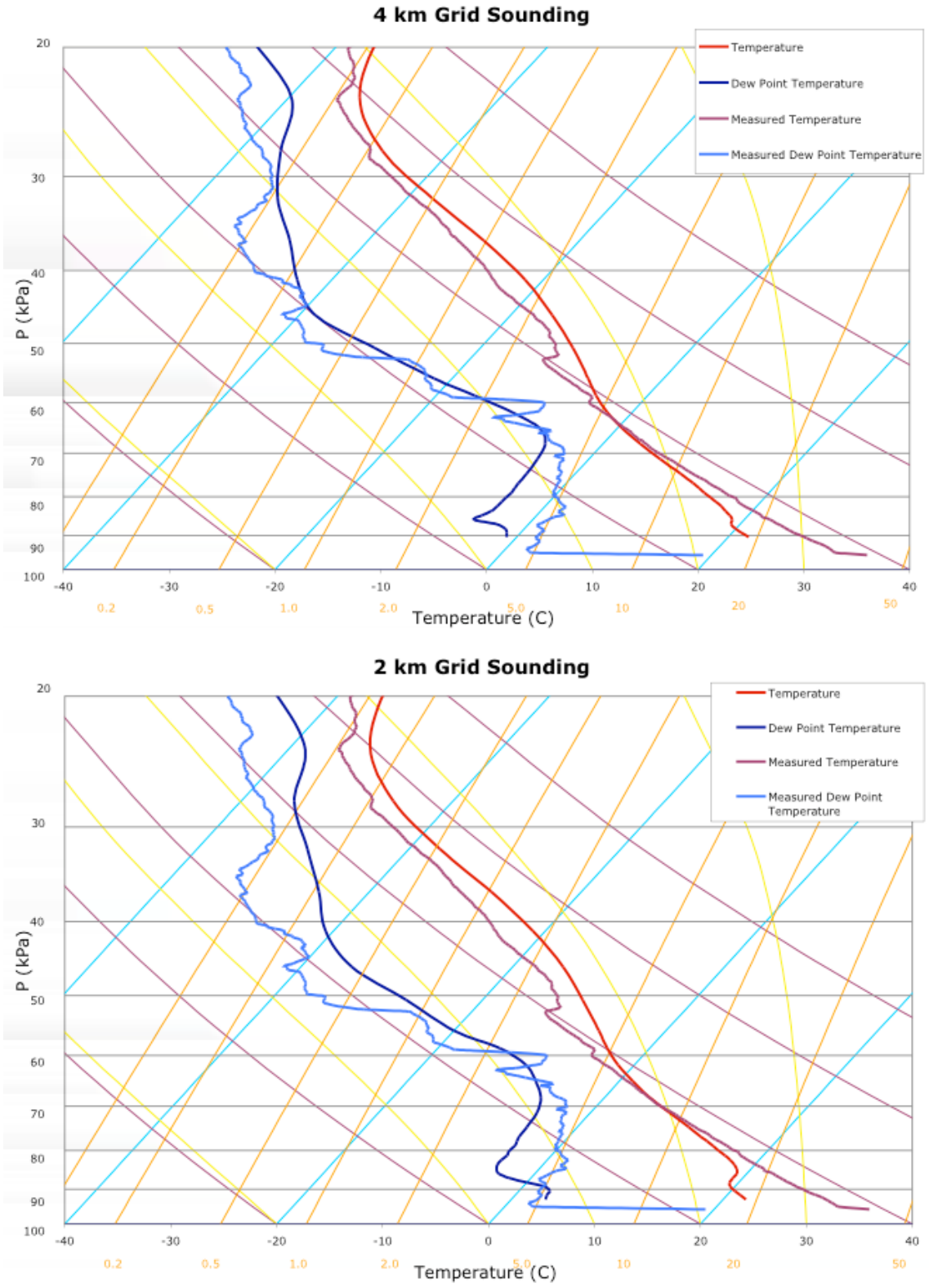

Fig. 1.7 a & b Forecast soundings produced by the 4 km grid and 2 km grid for Kelwona (49.93 N, 119.40 W, and, 456 m/MSL) from the 24 hour forecast of runs initialized at 00Z 14 June 2002, as well as the actual temperature and dew point temperature.